MODELING *KEPLER* TRANSIT LIGHT CURVES AS FALSE POSITIVES: REJECTION OF BLEND SCENARIOS FOR KEPLER-9, AND VALIDATION OF KEPLER-9 d, A SUPER-EARTH-SIZE PLANET IN A MULTIPLE SYSTEM

Guillermo Torres[1], François Fressin[1], Natalie M. Batalha[2], William J. Borucki[3], Timothy M. Brown[4],
Stephen T. Bryson[3], Lars A. Buchhave[5], David Charbonneau[1], David R. Ciardi[6], Edward W. Dunham[7],
Daniel C. Fabrycky[1], Eric B. Ford[8], Thomas N. Gautier III[9], Ronald L. Gilliland[10], Matthew J. Holman[1],
Steve B. Howell[11], Howard Isaacson[12], Jon M. Jenkins[13], David G. Koch[3], David W. Latham[1], Jack J. Lissauer[3],
Geoffrey W. Marcy[14], David G. Monet[15], Andrej Prsa[16], Samuel N. Quinn[1], Darin Ragozzine[1], Jason F. Rowe[3,19],
Dimitar D. Sasselov[1], Jason H. Steffen[17], and William F. Welsh[18]

[1] Harvard-Smithsonian Center for Astrophysics, Cambridge, MA 02138, USA; gtorres@cfa.harvard.edu
[2] San Jose State University, San Jose, CA 95192, USA
[3] NASA Ames Research Center, Moffett Field, CA 94035, USA
[4] Las Cumbres Observatory Global Telescope, Goleta, CA 93117, USA
[5] Niels Bohr Institute, Copenhagen University, DK-2100 Copenhagen, Denmark
[6] NASA Exoplanet Science Institute/Caltech, Pasadena, CA 91125, USA
[7] Lowell Observatory, Flagstaff, AZ 86001, USA
[8] University of Florida, Gainesville, FL 32611, USA
[9] Jet Propulsion Laboratory/California Institute of Technology, Pasadena, CA 91109, USA
[10] Space Telescope Science Institute, Baltimore, MD 21218, USA
[11] National Optical Astronomy Observatory, Tucson, AZ 85719, USA
[12] San Francisco State University, San Francisco, CA 94132, USA
[13] SETI Institute/NASA Ames Research Center, Moffett Field, CA 94035, USA
[14] University of California, Berkeley, CA 94720, USA
[15] US Naval Observatory, Flagstaff Station, Flagstaff, AZ 86001, USA
[16] Villanova University, Villanova, PA 19085, USA
[17] Fermilab Center for Particle Astrophysics, P.O. Box 500, Batavia, IL 60510, USA
[18] San Diego State University, San Diego, CA 92182, USA

ABSTRACT

Light curves from the *Kepler* Mission contain valuable information on the nature of the phenomena producing the transit-like signals. To assist in exploring the possibility that they are due to an astrophysical false positive, we describe a procedure (BLENDER) to model the photometry in terms of a "blend" rather than a planet orbiting a star. A blend may consist of a background or foreground eclipsing binary (or star–planet pair) whose eclipses are attenuated by the light of the candidate and possibly other stars within the photometric aperture. We apply BLENDER to the case of Kepler-9 (KIC 3323887), a target harboring two previously confirmed Saturn-size planets (Kepler-9 b and Kepler-9 c) showing transit timing variations, and an additional shallower signal with a 1.59 day period suggesting the presence of a super-Earth-size planet. Using BLENDER together with constraints from other follow-up observations we are able to rule out all blends for the two deeper signals and provide independent validation of their planetary nature. For the shallower signal, we rule out a large fraction of the false positives that might mimic the transits. The false alarm rate for remaining blends depends in part (and inversely) on the unknown frequency of small-size planets. Based on several realistic estimates of this frequency, we conclude with very high confidence that this small signal is due to a super-Earth-size planet (Kepler-9 d) in a multiple system, rather than a false positive. The radius is determined to be $1.64^{+0.19}_{-0.14}\ R_\oplus$, and current spectroscopic observations are as yet insufficient to establish its mass.

Key words: binaries: eclipsing – planetary systems – stars: individual (Kepler-9, KIC 3323887, KOI-377) – stars: statistics

Online-only material: color figures

1. INTRODUCTION

The *Kepler* Mission, launched in March of 2009, was designed to address the important question of the frequency of Earth-size planets around Sun-like stars, and to characterize extrasolar transiting planets through a 3.5 year program of very precise photometric monitoring of ∼156,000 stars (Koch et al. 2010). Science results from the mission have already begun to appear (Borucki et al. 2010, 2011; Steffen et al. 2010). As shown already by ground-based surveys for transiting planets,

considerable effort is required to validate candidates detected photometrically. This is because false positives usually outnumber true planetary systems by a large factor, which is about 10:1 for the most successful surveys from the ground, but is not yet well characterized for *Kepler*. The follow-up efforts by the *Kepler* team have been summarized by Batalha et al. (2010).

Spectroscopy is often a crucial step in the vetting process, as it allows not only to measure the mass of a planet but also to examine any changes in the line profiles (bisector spans) that might indicate a false positive (see Queloz et al. 2001; Torres et al. 2005). Some of the most challenging false positives to rule out include chance alignments with a background eclipsing

---

[19] NASA Postdoctoral Program Fellow.

Report Documentation Page

1. REPORT DATE **NOV 2010**	2. REPORT TYPE	3. DATES COVERED **00-00-2010 to 00-00-2010**

4. TITLE AND SUBTITLE	5a. CONTRACT NUMBER
Modeling Kepler Transit Light Curves as False Positives: Rejection of Blend Scenarios for Kepler-9, and Validation of Kepler-9 d, A Super-Earth-Size Planet in a Multiple System	5b. GRANT NUMBER
	5c. PROGRAM ELEMENT NUMBER
6. AUTHOR(S)	5d. PROJECT NUMBER
	5e. TASK NUMBER
	5f. WORK UNIT NUMBER

7. PERFORMING ORGANIZATION NAME(S) AND ADDRESS(ES) **California Institute of Technology,Jet Propulsion Laboratory/,Pasadena,CA,91125**	8. PERFORMING ORGANIZATION REPORT NUMBER

9. SPONSORING/MONITORING AGENCY NAME(S) AND ADDRESS(ES)	10. SPONSOR/MONITOR'S ACRONYM(S)
	11. SPONSOR/MONITOR'S REPORT NUMBER(S)

12. DISTRIBUTION/AVAILABILITY STATEMENT
Approved for public release; distribution unlimited

13. SUPPLEMENTARY NOTES

14. ABSTRACT
Light curves from the Kepler Mission contain valuable information on the nature of the phenomena producing the transit-like signals. To assist in exploring the possibility that they are due to an astrophysical false positive we describe a procedure (BLENDER) to model the photometry in terms of a ?blend? rather than a planet orbiting a star. A blend may consist of a background or foreground eclipsing binary (or star?planet pair) whose eclipses are attenuated by the light of the candidate and possibly other stars within the photometric aperture. We apply BLENDER to the case of Kepler-9 (KIC 3323887), a target harboring two previously confirmed Saturn-size planets (Kepler-9 b and Kepler-9 c) showing transit timing variations, and an additional shallower signal with a 1.59 day period suggesting the presence of a super-Earth-size planet. Using BLENDER together with constraints from other follow-up observations we are able to rule out all blends for the two deeper signals and provide independent validation of their planetary nature. For the shallower signal, we rule out a large fraction of the false positives that might mimic the transits. The false alarm rate for remaining blends depends in part (and inversely) on the unknown frequency of small-size planets. Based on several realistic estimates of this frequency, we conclude with very high confidence that this small signal is due to a super-Earth-size planet (Kepler-9 d) in a multiple system, rather than a false positive. The radius is determined to be 1.64+0.19 −0.14 R⊕, and current spectroscopic observations are as yet insufficient to establish its mass.

15. SUBJECT TERMS

16. SECURITY CLASSIFICATION OF:			17. LIMITATION OF ABSTRACT	18. NUMBER OF PAGES	19a. NAME OF RESPONSIBLE PERSON
a. REPORT **unclassified**	b. ABSTRACT **unclassified**	c. THIS PAGE **unclassified**	**Same as Report (SAR)**	**18**	

binary ("blends"). However, for faint candidates ($V > 14$) high-resolution, high signal-to-noise ratio (S/N) spectroscopy becomes prohibitively expensive in terms of telescope time. Even for brighter candidates, the reflex motion of the star due to an Earth-mass planet can sometimes be below the radial-velocity detection limit, making spectroscopic confirmation very difficult or impossible. The question then becomes how to validate these candidates, particularly the ones with small planets that are precisely among the most interesting.

A number of other tests have been developed that can aid in understanding the nature of the candidate, and that rely on the long-term and nearly continuous photometric monitoring of *Kepler*, as well as the very high astrometric precision achieved in determining the centroids of the stars (see also Steffen et al. 2010). These tests include: (1) verifying that alternating events have the same depth, which they may not if the signal is due to a background eclipsing binary; (2) checking for the presence of shallow secondary eclipses, which are common in eclipsing binaries but are not expected for the smallest planets; (3) checking for ellipsoidal variations, which could be another sign of a blend; (4) checking for changes in the centroid positions correlated with the brightness changes, which, if detected, might indicate a blend, or at the very least, a crowded aperture. This is a powerful diagnostic that is able to disprove many background blends.

In addition to these tests, high-resolution imaging is an important tool to identify neighboring stars that might be eclipsing binaries with the potential to cause the transit-like signals. The photometric aperture of *Kepler* is large enough (typically many arcseconds across) that it usually includes other stars in addition to the candidate, which increases the risk of such blends. In some cases, near-infrared observations with Warm *Spitzer* can allow one to reject the planet hypothesis if the transit depth at 3.6 μm or 4.5 μm is significantly different from that in the *Kepler* band. Such a signature might result from a blend with an eclipsing binary of a different spectral type than the candidate.[20]

Even with this extensive battery of tests it may still be difficult or impossible to provide validation for many of the most interesting planet candidates discovered by *Kepler*. For example, blend scenarios involving an eclipsing binary or an eclipsing star–planet pair physically associated with the candidate (hierarchical triple systems) and in a long-period orbit around their common center of mass would often be spatially unresolved from the ground. These configurations may also not be detectable spectroscopically, and would likewise not produce any measurable centroid motion. Therefore, it is imperative to take advantage of all the information available in vetting candidates.

With this as our motivation, we describe here the use of the *Kepler* light curves themselves in a different way to help discriminate between true planetary transits and a large variety of possible blend scenarios, on a much more quantitative basis than simple back-of-the-envelope calculations could provide. The technique tests these scenarios by directly modeling the light curves as blends and has considerable predictive power that allows the expected properties of the various configurations to be tested against other information that may be available. Both hierarchical triples and background blends can be explored. A restricted application of this type of modeling to *Kepler*

has already been made for the five multi-planet candidates announced recently by Steffen et al. (2010). For the present paper we have chosen to illustrate the full potential of the method, which we refer to as BLENDER, by applying it to the unique case of *Kepler* Object of Interest 377 (KOI-377, henceforth Kepler-9). This is a multi-planet system reported and described in detail by Holman et al. (2010), with *three* low-amplitude periodic signals in its light curve. We have selected this system for two main reasons. On the one hand, it represents the first unambiguous detection of transit timing variations (TTVs) in an extrasolar planet, with a pattern of variation seen in two of its signals (Kepler-9 b and Kepler-9 c) that constitutes irrefutable evidence that the objects producing them are bona fide planets. This offers an ideal opportunity to test BLENDER because their true nature is already known. On the other hand, the third signal (KOI-377.03)[21] is small enough that it would correspond to a super-Earth, but validation of its planetary origin is not yet in hand. Should it be validated, Kepler-9 would become an even more remarkable laboratory for the study of the architecture of planetary systems involving small planets. Thus, exploring the wide range of possible blend configurations that might mimic this shallow signal is of the greatest interest for determining its true nature.

Kepler is likely to find many other candidate transiting planets similar to KOI-377.03, for which final validation by other means is not currently feasible, either because the expected radial-velocity signal is too small or because Doppler measurements are otherwise complicated due to the star being chromospherically active, rapidly rotating, or too faint. With the application to Kepler-9 we show that our light-curve modeling technique is a powerful tool for exploring astrophysical false positive scenarios that is complementary to other diagnostics, and should play an important role in the discovery of Earth-size planets around other *Kepler* targets.

2. SIMULATING FALSE POSITIVES WITH BLENDER

In general the detailed shape of a light curve displaying transit-like events can be expected to contain useful constraints on possible blend scenarios that might be responsible for those signals. With photometry of the quality of that provided by *Kepler*, those constraints can be quite strong and may be used to exclude many blend configurations and provide support for the planetary hypothesis. It is thus highly desirable to take advantage of this information, particularly since it relies only on observations already in hand.

The idea behind BLENDER is to compare the transit photometry of a candidate against synthetic light curves produced by an eclipsing binary that is included within the photometric aperture of *Kepler*, and is contaminating the light of the candidate. The usually deep eclipses of the binary are attenuated by the light of the candidate, and reduced in depth so that they appear transit-like. In principle there is an enormous range of possible binary configurations that could mimic all of the features of true planetary transits, including not only their depth, but also the total duration and the length of the ingress and egress phases. Generally, it is only with detailed modeling that these can be ruled out. Possible scenarios include not only background eclipsing binaries, but also hierarchical triples, i.e., an eclipsing

---

binary physically associated with the candidate in a wide orbit around their common center of mass.

The basic procedure for simulating light curves with BLENDER was described in detail by Torres et al. (2004), and further changes and enhancements are discussed below. Briefly, the brightness variations of an eclipsing binary are generated with the binary light-curve code EBOP (Popper & Etzel 1981), based on the Nelson–Davis–Etzel model (Nelson & Davis 1972; Etzel 1981), and then diluted by the light of the candidate for comparison with the *Kepler* observations. Effects such as limb darkening, gravity brightening, mutual reflection, and oblateness of the binary components are included. The objects composing the binary are referred to as the "secondary" and "tertiary," and the candidate is the "primary." The properties of each object needed to generate the light curves (brightness and size) are taken from model isochrones by Marigo et al. (2008), parameterized in terms of their stellar mass.[22] For the primary star the appropriate isochrone is selected by using as constraints the effective temperature, surface gravity, and metallicity determined spectroscopically. We assign also a mass and a radius from this isochrone, although these characteristics are irrelevant for generating the model light curves. We then read off the intrinsic brightness of the star (absolute magnitude) in the *Kepler* passband, which is the only property needed by BLENDER. The brightness of the primary is held fixed throughout all simulations. The parameters of the binary components are allowed to vary freely over wide ranges in order to provide the best match to the *Kepler* photometry in a χ^2 sense, subject only to the condition that the two stars lie on the same isochrone, as expected from coeval formation. To read off their properties (absolute magnitude and size) we use the mass as an intermediate variable. The specific isochrone adopted for the binary depends on the configuration: for hierarchical triple scenarios we adopt the same age and chemical composition as the primary, whereas for background binaries the isochrone can be different. The *Kepler* light curve itself does not provide a useful constraint on the age or metallicity of the binary in the background case, so a typical choice is a model for solar metallicity and a representative age for the field such as 3 Gyr. For background binary scenarios the distance between the binary and the main star is parameterized for convenience in terms of the difference in distance modulus, $\Delta\delta$. The inferred distance between the primary star and the observer will vary from blend to blend because we constrain the combined brightness of all components of the blend to match the measured apparent brightness of the target. BLENDER is also able to account for differential extinction between the primary and the binary, which can have a non-negligible effect in some cases given the relatively low Galactic latitude of the *Kepler* field.

Early versions of BLENDER have been used occasionally in recent years to examine transiting planet candidates from ground-based surveys such as OGLE, TrES, and HATNet (see, e.g., Torres et al. 2004, 2005; Mandushev et al. 2005; O'Donovan et al. 2006; Bakos et al. 2007), as well as from *CoRoT* (F. Fressin et al. 2011, in preparation). These studies have exploited the predictive power of BLENDER to estimate further properties of the blend scenarios, by testing them against

complementary information such as color indices, optical/near-infrared spectroscopy, or near-infrared photometry from *Spitzer*. For the application to *Kepler*, several important modifications have been made to BLENDER, including the following: (1) the ability to generate light curves integrated over the 29.4 minute effective duration of an observation when using long-cadence data. This changes the shape of the transits significantly, given the high precision of the *Kepler* photometry and the relatively short timescales of the events (see Gilliland et al. 2010; Kipping 2010); (2) de-trending of the original *Kepler* light curves with a 1 day running median to remove instrumental effects, and rejection of outliers; (3) the use of model isochrones specific to the *Kepler* passband, kindly computed for us by L. Girardi. BLENDER can now also use proper limb-darkening coefficients for the same band, as opposed to an approximation to the *Kepler* passband such as the Johnson *R* filter, which is considerably narrower. *Kepler* limb-darkening coefficients have been computed by Sing (2010) and also A. Prsa;[23] (4) extension to any optical or near-infrared passband. In particular, for any scenario explored with BLENDER, light curves can be computed at other wavelengths such as the 3.6 μm and 4.5 μm passbands of the IRAC instrument on Warm *Spitzer*, in order to further test the blend hypothesis. Additionally, BLENDER can predict the overall color of a blend in any pair of passbands, including the effects of differential reddening for background or foreground scenarios. These colors may then be compared with the measured colors of a target. Extinction at different wavelengths is computed following the prescription by Cardelli et al. (1989); (5) the ability to have the tertiary be a (dark) planet instead of a star, in which case the corresponding free parameter becomes the radius of the planet rather than the tertiary mass. The mass of the planet has little effect on the light curves in most cases, but can nevertheless be set to any value;[24] (6) the ability to include extra light from other stars that may be present in the *Kepler* aperture, which further dilutes the intrinsic signatures from the eclipsing binary; (7) the ability to model systems with eccentric orbits. Eccentricity changes the orbital velocities during transit, and can therefore affect the size (mass) of stars that allow satisfactory fits to the light curve.

When exploring blend scenarios involving hierarchical triple systems, the free parameters of the problem are the mass of the secondary, the mass of the tertiary (or its radius, if a planet), and the inclination angle. A fourth variable, the difference in distance modulus, is added for background blends. These quantities are typically stepped over wide ranges in a grid pattern to fully map the χ^2 surface. For the application to Kepler-9 below, stellar masses are allowed to vary along the isochrones between 0.1 $M_\odot$ and 1.4 $M_\odot$, although at the larger values the observed duration of the transits is already difficult to match unless the events are highly grazing, in which case the shape would be very different. For planetary tertiaries the radii are allowed to be as large as 1.8 $R_{\rm Jup}$; values higher than this have not been observed.

3. APPLICATION TO KEPLER-9

Kepler-9 (KIC 3323887, 2MASS 19021775+3824032) is a relatively faint star compared to typical ground-based

---

[22] This particular set of isochrones was chosen because it reaches lower masses than other models (nominally 0.15 $M_\odot$, which we have extrapolated slightly for this application to 0.10 $M_\odot$, near the brown dwarf limit), and because a convenient web tool provided by the authors allows easy interpolation in both age and metallicity (http://stev.oapd.inaf.it/cgi-bin/cmd). Additionally, isochrone magnitudes are available in a variety of passbands including the *Kepler* and *Spitzer* passbands, as well as Sloan and 2MASS.

[23] http://astro4.ast.villanova.edu/aprsa/?q=node/8
[24] We note that this option of BLENDER implicitly allows to consider white dwarfs as tertiaries, as they are also Earth-size and contribute little light. Their mass is significantly larger than a planet's mass, however, which in close orbits can lead to distortions in the primary star causing ellipsoidal variation. Gravitational microlensing may also occur in systems involving white dwarfs with long enough periods, and may well be detectable in the *Kepler* photometry.

transit hosts (*Kepler* magnitude $Kp = 13.8$), which was observed by the mission beginning in the first quarter of operations, and presents three distinct periodic signals in its light curve. The two with the largest amplitudes have periods of 19.24 days (Kepler-9 b) and 38.91 days (Kepler-9 c), and brightness decrements of 6.5 and 6.0 mmag, respectively. The third signal (KOI-377.03) is much shallower (0.2 mmag) and repeats every 1.59 days. The two longer periods are within 2.5% of being in a 2:1 ratio, and both objects display obvious TTVs that are anti-correlated, clearly indicating they are interacting gravitationally and therefore orbit the same star, and are planetary in nature (see Holman et al. 2010). The estimated radii are quite similar to that of Saturn, and the masses are somewhat smaller than Saturn, based on available radial-velocity measurements constrained by transit times and durations. The short-period signal has one of the smallest amplitudes detected by *Kepler*, and may well correspond to a third, super-Earth-size planet in the system, with an estimated radius of only $\sim$1.5 $R_\oplus$ (Holman et al. 2010). However, because it shows no TTVs related to the other two planets (nor is expected to, on dynamical grounds), and is predicted to induce only a very small reflex velocity on the parent star that may be below detection for such a faint object, the true origin of this signal has not yet been established.

In the absence of the crucial evidence of TTVs, each of the two largest signals—and indeed the third signal as well—could in principle be due to a different blend.[25] Therefore, as an illustration of the application of BLENDER, we model the light curve of Kepler-9 at each period separately, as we would any candidate with a single period, and we account for possible blends at the other periods by incorporating extra dilution consistent with those other scenarios. The goal for the two largest signals is to demonstrate, as a sanity check, that BLENDER would be able to rule out blends in similar cases where confirmation is lacking, which *Kepler* is expected to find in significant numbers. For the third signal of unknown nature, the application of BLENDER should provide valuable evidence one way or the other.

3.1. Stellar Properties and Photometry

Kepler-9 is a solar type star. The spectroscopic properties of the primary are adopted from Holman et al. (2010): $T_{\rm eff} = 5777 \pm 61$ K, $\log g = 4.49 \pm 0.09$, and [Fe/H] $= +0.12 \pm 0.04$. With these parameters, a comparison with the stellar evolution models of Marigo et al. (2008) yields a stellar mass of $M_\star = 1.07 \pm 0.05\ M_\odot$, a radius of $R_\star = 1.02 \pm 0.05\ R_\odot$, and an age of about 1 Gyr, along with the absolute magnitude in the *Kepler* band. Only the latter is used by BLENDER and is held fixed in our modeling. The distance to the star estimated from the same models is about 650 pc, ignoring extinction. Uncertainties in the brightness of the primary stemming from errors in $T_{\rm eff}$, $\log g$, and [Fe/H] are small. For example, the error in $\log g$, which has the most direct influence on the intrinsic brightness, translates to an uncertainty of little more than 0.1 mag in the absolute magnitude. This has an insignificant impact on our results.

The photometry used here consists of the long-cadence measurements gathered for Kepler-9 during *Kepler* quarters 1, 2, and 3, spanning 218 days, and was treated slightly differently than indicated earlier for a generic *Kepler* candidate because of the complications stemming from the TTVs. Using the binary FITS tables from MAST (Multimission Archive at STScI, http://archive.stsci.edu/kepler/), the "raw" aperture photometry for each quarter was first de-trended using a moving cubic polynomial fit robustly to out-of-transit data, with a sliding window of 999 minutes before and after each individual datapoint. This technique removes long-term trends due to stellar activity or instrumental errors, but retains the properties of each transit light curve. Statistically significant outliers were removed.

For the two long-period signals, simple folding will not create an accurate light curve because of the strong TTVs. Instead, we used a "shift-and-stack" technique, in which each transit event is displaced so that it is centered at "time" zero using the measured transit times from Holman et al. (2010). Along with the measurements in transit, nearly a full cycle of out-of-transit data was also shifted. Specifically, we shifted nearly 25% of an orbital cycle before the transit, and nearly 75% after the transit. This preserves any curvature outside of eclipse, and in principle would also retain any secondary eclipses, both of which can provide useful constraints when modeling the light curve with BLENDER. We note, however, that the strong TTVs would be accompanied by shifted secondary eclipses in a way that can only be predicted by full numerical integration. This shift-and-stack technique would not align secondary eclipses correctly and thus their depth would need to be significant in each individual event to be noticed. There is no sign of secondary eclipses at these periods in the data at the 10^{-4} level, as expected from the planetary nature of the objects, and thus the failure of the shift-and-stack technique to correctly add up the secondary eclipses does not affect our results. After shifting, all the transit and out-of-transit data were "stacked" together and each data point was given a time relative to time zero at the center of each transit event. This was done separately for the 19 day and 39 day signals. We have been careful not to use a full cycle of out-of-transit data to avoid using any photometric measurements more than once in the input light curve.

For the 1.6 day signal that repeats at regular intervals (since it shows no TTVs), we created a light curve by simply masking out the transits at the other two periods.

3.2. Additional Observations for False Positive Rejection

The photometric aperture of *Kepler* is typically a few pixels across, with a scale of $3\rlap{.}''98$ per pixel (see below). High-resolution imaging of Kepler-9 was performed in order to identify neighboring stars that might be eclipsing binaries blended with and contaminating the target photometry. Images were recorded with the guider camera of the High Resolution Echelle Spectrometer (HIRES; Vogt et al. 1994) on the Keck I telescope on Mauna Kea, in unfiltered light. The nominal sensitivity of the CCD from 400 to 800 nm yields an effective passband similar to the *Kepler* passband. The field of view was $43'' \times 57''$, and the pixel scale was $0\rlap{.}''30$ per pixel. One of these frames appears in Figure 1 and shows at least four stars in the field of view within $15''$ of the target. Some of these stars are listed in various astrometric and photometric catalogs. The brightness of these companions relative to the target was measured using aperture photometry on four separate Keck images and ranges from $\Delta m = 2.6$ to 5.9 mag.

---

[25] Unlikely as it may seem to have three different blends operating in the same system, the large photometric aperture, nearly uninterrupted monitoring, very high photometric precision, and long-term coverage of *Kepler* coupled with the large number of targets observed makes it more sensitive to picking up odd cases such as this, so they should not be completely ruled out. An example already exists among the five multi-planet candidates recently reported by Steffen et al. (2010), in which one of the systems (KOI-191) presents three transit-like signals, and one of those signals (0.4 mmag depth) has been shown to be due to a background eclipsing binary 2.6 mag fainter than the target, located 1.5 arcsec away.
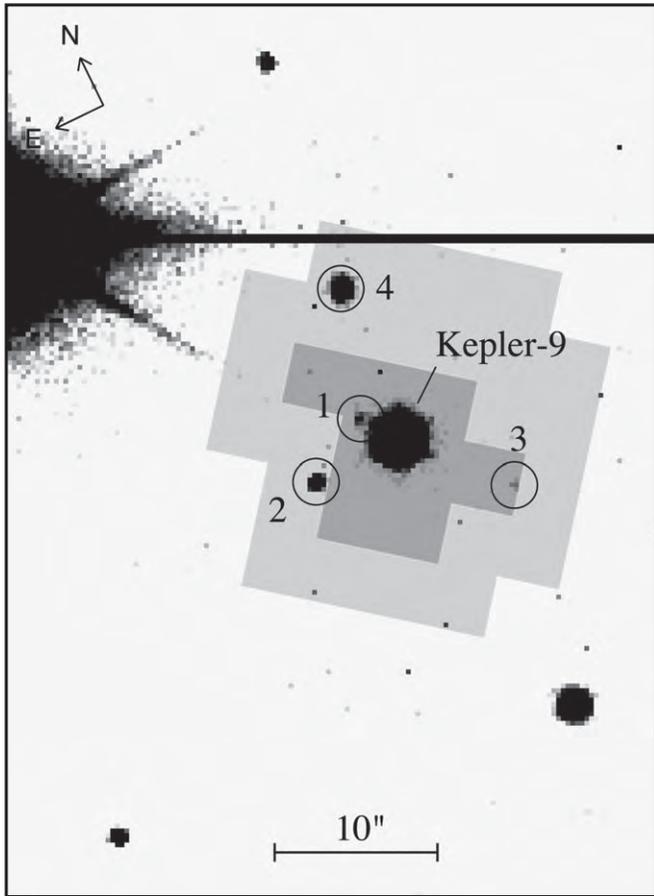
Figure 1. Image of Kepler-9 from the HIRES guider camera on the Keck I telescope, obtained in seeing of $0\farcs9$ and clear skies. Companions within $15''$ are labeled as in Table 1. The scale of the image is $0\farcs30$ pixel^{-1}. Also indicated are the optimal photometric aperture (darker gray area of 8 pixels, used to extract the *Kepler* photometry) and the target aperture mask (lighter gray area of 31 pixels, used to measure centroids) for *Kepler* quarter 3.
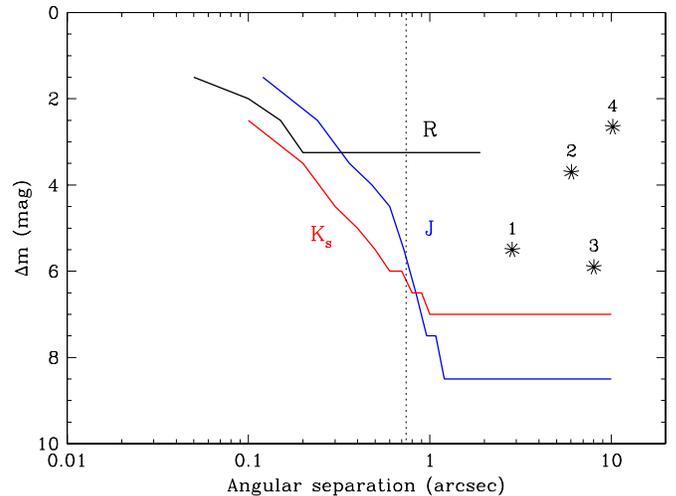

Figure 2. Sensitivity to faint companions near Kepler-9 from our imaging observations. Any companions above the curves are bright enough to be detected. J and K_s limits are from AO observations at the Palomar 200 inch telescope, and R is from speckle observations using the WIYN 3.5 m telescope. Companions to the right of the vertical dotted line at $0\farcs74$ cannot be responsible for the 1.6 day signal, as they would have induced centroid motion that is not observed. Stars detected in our imaging observations (Table 1) are marked with asterisks at their measured angular separations and magnitude differences in the *Kepler* passband.

(A color version of this figure is available in the online journal.)

Table 1
Companions to Kepler-9 Identified in our Imaging Observations

Identification	SDSS Coordinates (J2000)	ρ ($''$)	P.A. (deg)	ΔJ (mag)	ΔK_s (mag)	ΔKp (mag)
Kepler-9[a]	19:02:17.76 +38:24:03.2	...	...	...	...	...
Comp 1[b]	19:02:17.91 +38:24:05.4	2.85	37.9	6.84	6.84	5.5
Comp 2	19:02:18.27 +38:24:02.8	6.04	91.7	4.52	4.17	3.7
Comp 3	19:02:17.29 +38:23:57.1	8.03	221.8	6.25	6.04	5.9
Comp 4[c]	19:02:17.69 +38:24:13.4	10.21	355.6	3.59	3.01	2.6

Notes.
[a] Target is also known as 2MASS 19021775+3824032 and KIC 3323887.
[b] This companion is not listed in the SDSS catalog; the coordinates are inferred from its position relative to Kepler-9.
[c] Also known as 2MASS 19021769+3824132 and KIC 3323885.

Speckle observations of Kepler-9 were carried out on 2010 June 18 with the WIYN 3.5 m telescope located on Kitt Peak. They were taken with a two-color EMCCD speckle camera using narrow-band filters 40 nm wide centered at 562 nm and 692 nm. We refer loosely to these passbands as V and R. The native seeing was $0\farcs7$. No companions with $\Delta m \leqslant 3.25$ mag (R band) are present in the field of view centered on the target out to $1\farcs8$, at the 5σ confidence level. Inside of $0\farcs2$ the sensitivity is reduced, but still allows to rule out brighter companions down to the diffraction limit of $0\farcs04$–$0\farcs05$ (see Figure 2). Details of the follow-up speckle observations in the context of the *Kepler* Mission are described in more detail by S. Howell et al. (2011, in preparation).

Additionally, Kepler-9 was observed on 2010 July 2 at the Palomar Hale 200 inch telescope with the near-infrared adaptive optics (AO) PHARO instrument (Hayward et al. 2001), a 1024×1024 Rockwell HAWAII HgCdTe array detector. Observations were made in the J (1.25 μm) and K_s (2.145 μm) bands. The field of view was approximately $20'' \times 20''$, and the scale was 25.1 mas per pixel. The AO system guided on the primary target itself, and produced Strehl ratios of 0.05 at J and 0.3 at K_s. The central cores of the resulting point-spread functions had widths of FWHM $= 0\farcs12$ at J and FWHM $= 0\farcs10$ at K_s. The closer of the companions seen earlier in the Keck images were easily detected, and we list them all

in Table 1 along with relative positions (angular separations and position angles), relative brightness estimates, and other identifications. The sensitivity to faint companions was studied by injecting artificial stars into the image at various separations and with a range of Δm, and then attempting to detect them both by eye and with an automated IDL procedure based on DAOPHOT. For firm detection we required the artificial stars to be present in both passbands. The sensitivity curves as a function of angular separation are shown in Figure 2, along with the R-band sensitivity estimated from the speckle observations.

Much fainter stars with $\Delta m > 9$ near a *Kepler* target could in principle be detected by examining images from the Palomar Observatory Sky Survey, which date back more than 50 years, provided the proper motion of the target is large enough to have shifted it by several arcseconds over that period. This is not possible for Kepler-9, since its total proper motion as reported in the UCAC2 Catalog (Zacharias et al. 2004) is only 13.7 mas yr^{-1}. The likelihood of such faint close-in companions must therefore be addressed statistically, if need be.

While the AO and speckle observations rule out the presence of bright neighboring stars as close as $0\farcs1$ or slightly less, further limits on even tighter companions can be placed by

the spectroscopic observations obtained with HIRES on the Keck I telescope, described by Holman et al. (2010), since those stars would fall well within the 0″.86 slit of the spectrograph. We performed simulations in which we added the spectrum of a faint star to the original Kepler-9 spectra, over a range of relative brightnesses, and attempted to detect these artificial companions by examining the cross-correlation function. We estimate conservatively that any such stars with relative fluxes larger than about 10%–15% (Δm less than 2–2.5 mag) would have been seen, unless their spectral lines are blended with those of the target. The sharp lines of Kepler-9, with a measured rotational broadening of only $v \sin i = 1.9 \pm 0.5$ km s^{-1}, make this rather unlikely.

3.3. Centroid Analysis

Thanks to the very high astrometric precision of *Kepler*, an analysis of the motion of the photocenter of a target provides an effective way of identifying false positives that are caused by background eclipsing binaries falling within the aperture. The principles have been explained by Batalha et al. (2010) (see also Jenkins et al. 2010; Monet et al. 2010). The centroid measurements described below use data from quarter 3 only. In quarter 1 the Kepler-9 aperture was determined to be too small to optimally capture its flux and was subsequently enlarged. In quarter 2 *Kepler* experienced undesirable pointing drift, which was later resolved. These problems complicate the centroid analysis for quarters 1 and 2, although the results are broadly consistent with the more reliable ones from quarter 3 presented here.

We describe first the use of difference image analysis to demonstrate that the transit sources for all three Kepler-9 planets and candidates are restricted to being very near the target star. A difference image is formed by averaging several exposures near, but outside of a transit and subtracting from this the average of all available exposures near transit center. This results in a typically isolated signal, a positive intensity with the shape of the point-spread function (PSF) at the *true spatial location* of the transit source, and an amplitude equal to the photometric transit depth times the direct image intensity for the target. Adopting 40 independent transits of KOI-377.03 in quarter 3 (avoiding those shortly after major disturbances such as a safing event, and avoiding any that overlap with "b" and "c" transits), each formed with six symmetrically placed exposures outside of transits (after a two exposure gap) and three near transit minimum, results in a 14σ signal in the difference image. The corresponding direct image is formed as the average of both in- and out-of-transit sets such that the direct and difference images are sums and differences of precisely the same exposure sets.

For Kepler-9 b four transits were used from quarter 3 with five exposures in transit, a gap of three, then five more exposures on each side for out-of-transit. Kepler-9 c used two transits with seven exposures in-transit, a gap of three, and seven symmetrically placed out-of-transit exposure blocks. By using only exposures pulled close in time, and symmetrically with respect to the transits in use to form a difference image, this effectively imposes a de-trending and avoids any complications from drifts on timescales longer than the average spread of the out-of-transit sets, which for Kepler-9 c (the widest) is about 9 hr. Inspection of the difference images in Figure 3 shows that the transit sources for the confirmed "b" and "c" planets (Holman et al. 2010) and the candidate KOI-377.03 must arise from close to the target star, with offsets approaching 1 pixel easily ruled out by inspection. A weighted PSF fit (or more
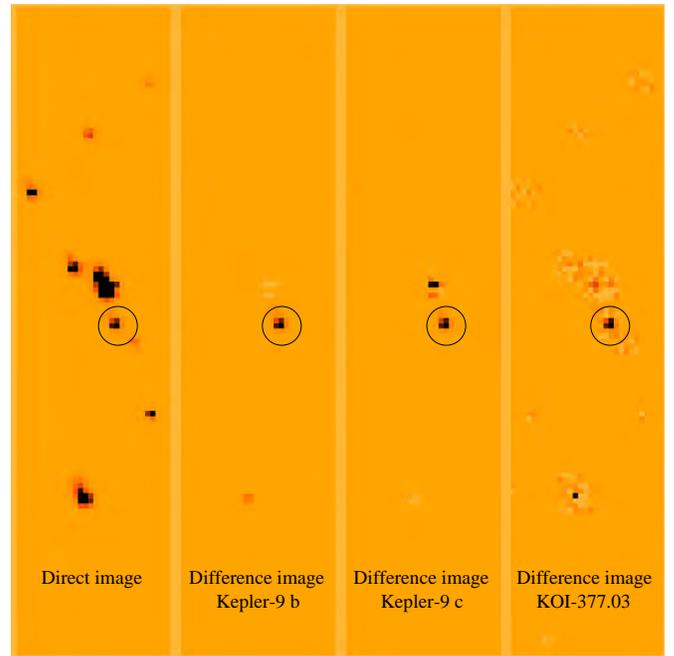

Figure 3. Direct and difference images for Kepler-9. The four panels from left to right show 128 (row) by 30 (column) regions corresponding to the direct and difference images for planets "b" and "c," and candidate KOI-377.03. The pixels returned for all stars in this area have been mapped into original row and column locations on the detector. Over 90% of the image area is unfilled since *Kepler* returns only postage stamps on stars of interest. The target (KIC 3323887) is indicated with circles in each panel. The locally brightest pixel is always at column 1100 and row 273, and each display panel has been normalized by the sum of counts within the 3 × 3 pixels centered on [1100, 273]. The display range is −0.03 to 0.3. The difference images were created to isolate the signals for transits "b," "c," and 377.03, respectively. Most stars, not having variations synced with these phases, effectively disappear in the difference images. For each of the three sets of transits the difference image in the 3 × 3 pixel core appears nearly identical to the direct image, demonstrating that the true transit source must be near the target to a small fraction of a pixel. The difference images also reflect the expected count levels for the source to be coincident with the target.

(A color version of this figure is available in the online journal.)

properly, a Pixel Response Function (PRF) fit; see Bryson et al. 2010) to each of the direct and three difference images of Figure 3 is formed using only the central 3 × 3 pixel area centered on the brightest pixel. This leads to offsets with respect to "b," "c," and KOI-377.03 of 0.007, 0.035, and 0.047 pixels, respectively. For KOI-377.03 the formal error from a weighted least-squares fit is 0.062 pixels. We have further assessed the errors by generating a large number of independent realizations of a transit signal of the KOI-377.03 relative intensity centered on the target coordinates. This leads to an rms scatter of 0.062 pixels. The noise had been increased by a factor of 1.2 in the difference image beyond direct Poisson plus readout noise estimates in order to yield this congruence of least-squares errors and scatter in simulations. The distribution of offsets follows expected Gaussian statistics, e.g., in the 7472 trials for KOI-377.03 the extreme offset is 4.2σ compared to the expected 4.0. We have also shown that simulating transit signals at 0.5 and 1.0 pixel offsets from the target results in similar and smaller statistical scatter, respectively, as less Poisson noise is under the transit image. We take the scatter of 0.062 pixels to generate a 3σ error circle of 0.186 pixels or 0″.74. This is the minimum radius within which background eclipsing binaries cannot be safely ruled out from centroid analysis of the *Kepler* data itself. To place this in perspective: centroid analysis has ruled out

Table 2
PRF Centroid Measurements on Kepler-9 Direct and Difference Images

Type	Intensity (e^-)	Column (pixel)	Row (pixel)	Radius Offset (pixel)
		Kepler-9 b		
Direct	5.170×10^7	1099.6989	273.4557	
Difference	4.360×10^5	1099.7058	273.4584	
S/N; Offset	174	0.0069	0.0027	0.0074
Errors	2506	0.0029	0.0039	0.0049
		Kepler-9 c		
Direct	5.132×10^7	1099.6999	273.4654	
Difference	3.833×10^5	1099.7107	273.4990	
S/N; Offset	128	0.0108	0.0336	0.0353
Errors	2991	0.0039	0.0056	0.0068
		KOI-377.03		
Direct	5.401×10^7	1099.6946	273.4408	
Difference	1.493×10^4	1099.7131	273.4836	
S/N; Offset	14.3	0.0185	0.0428	0.0047
Errors	1046	0.0351	0.0511	0.0062

Notes. The first two lines of each block present intensity and two coordinate position PRF fit results for the direct and difference images, respectively. The third line shows the photometric signal-to-noise for the intensity in the difference image, then the offset in position of the preceding two lines, with the last entry being the quadrature sum of the column and row offsets. Errors refer to the PRF fit to the difference image. The scale is 1 pixel = 3″.98.

98.6% of the area within the 8 pixel optimal aperture (>99.6% of the 31 pixel mask) of Figure 1 as the location of potential background eclipsing binaries creating the KOI-377.03 signal.

The quantitative results for all three transit sets are given in Table 2. Kepler-9 b shows an offset of 0.0074 pixels between the difference and direct image relative to a 1σ error of 0.0049 pixels. A 3σ error circle in which background binaries cannot be excluded from the centroid analysis of *Kepler* data itself is only 0″.06. Kepler-9 c is the only case of the three showing a formal inconsistency with the offset being 5σ; however, even if we combine the offset and 3σ formal error any background eclipsing binaries outside of a radius of 0″.22 are excluded as the transit signal source. Clearly for all three transit sets, with the 3σ error circles comfortably under 1″, all of the known companions from high-resolution imaging shown in Table 1 are safely ruled out as sources of the photometric transit signal. It is worth noting that the formal (and equal to scatter from Monte Carlo simulations) error on radial offsets is approximately equal in pixel units to the inverse photometric S/N, as expected (see, e.g., King 1983).

Further confirmation that at least the two deeper signals seen in Kepler-9 are not due to known stars in the scene can be obtained by placing simulated eclipses on the known stars in the aperture and comparing them with the observations. The scene in the aperture is modeled using stars in the *Kepler* Input Catalog (KIC; Latham et al. 2005), supplemented by the stars in Table 1. All stars within a PRF size (15 pixels) in row or column of Kepler-9's aperture are included. To generate the modeled out-of-transit image, the measured PRF is placed at each star's location on the focal plane, scaled by that star's flux. This provides the contribution of each star to the flux in the aperture's pixels. For each star s_i in the aperture, the depth d_{s_i} of a transit is computed that reproduces the observed depth in the aperture pixels. An in-transit image for each s_i is created as in the out-of-transit image, but with the flux of s_i suppressed by

$1 - d_{s_i}$. These model images are subject to errors in the PRF (Bryson et al. 2010), so they will not exactly match the sky.

A flux-weighted centroid is computed for the out-of-transit image and the in-transit-image generated for each star in the aperture. This produces row and column centroid offsets ΔR and ΔC, and the centroid offset distance $D = \sqrt{\Delta R^2 + \Delta C^2}$.

To compare these modeling results with observation we must make low-noise centroid measurements from the observed pixel data. We do this by creating out-of-transit and in-transit images from de-trended, folded pixel time series. For each pixel time series, the de-trending operation has three steps: (1) removal of a median-filtered time series with a window size equal to the larger of 48 cadences or three times the transit duration, (2) removal of a robust low-order polynomial fit, and (3) the application of a Savitzky–Golay filtered time series of order three with a width of 10 cadences. The Savitzky–Golay filter is not applied within 2 cadences of a transit event, so the transits are preserved. The resulting pixel time series are folded with the transit period. Each pixel in the out-of-transit image is the average of 30 points taken from the folded time series outside the transit, 15 points on either side of the transit event. Each pixel in the in-transit image is the average of as many points in the transit as possible: seven for Kepler-9 b and Kepler-9 c and four for KOI-377.03. Centroids are computed for the in-transit and out-of-transit images in the same way as the modeled images.

Uncertainties of these centroids are estimated via Monte Carlo simulation, where a noise realization is injected into 48 cadence smoothed versions of the pixel time series for each trial. A total of 2000 trials are performed each for Kepler-9 b, Kepler-9 c, and KOI-377.03. The in-transit and out-of-transit images are formed using the same de-trending, folding, and averaging as the flight data. The measured uncertainties are in the range of a few times 10^{-5} pixels.

Table 3 shows the resulting measurements of the centroids from quarter 3 pixel data, along with the Monte Carlo based 1σ uncertainties. The centroids are converted into centroid offsets and offset distance with propagated uncertainties. Table 4 shows the offset distance D predicted by the modeling method described above for each target in the aperture. We see that when the transit is on Kepler-9 itself we expect a measurable centroid shift for Kepler-9 b and Kepler-9 c. In this case the modeled centroid shift is about 3.7 times larger than that observed, though the signs of the offsets agree. This exaggeration of the centroid offset has been traced to inaccuracies in the KIC used to create the model images. Therefore, the centroid shifts in Table 4 should be scaled by a factor 1/3.7. If the transit were on one of the companion stars in the aperture, then the modeled centroid shift would be an order of magnitude larger than observed for Kepler-9 b and Kepler-9 c, ruling out the companion stars as the source for these signals. Companion stars are not as definitively ruled out for the KOI-377.03 transit by this technique. After scaling the centroid offsets as above, modeled transits on companions 3 and 4 have offsets that are about 2.5σ, while companion 2 is 1.9σ and companion 1 is less than 1σ. The modeled transit on Kepler-9, however, is much smaller, consistent with the observed transit offset for KOI-377.03.

3.4. BLENDER *Analysis of Kepler-9 b and c*

As an initial test, we modeled the light curves for each of these two signals assuming that they are the result of an eclipsing binary physically associated with the target, i.e., at the same distance (hierarchical triple). For this case the isochrone for the binary was taken to be the same as that of

Table 3
Observed Centroid Shifts for Kepler-9 b, Kepler-9 c, and KOI-377.03

	Kepler-9 b	Kepler-9 c	KOI-377.03
ΔR	$2.52 \times 10^{-4} \pm 7.78 \times 10^{-5}$	$1.65 \times 10^{-4} \pm 9.34 \times 10^{-5}$	$-1.24 \times 10^{-7} \pm 6.19 \times 10^{-5}$
ΔC	$-2.23 \times 10^{-4} \pm 7.55 \times 10^{-5}$	$-2.40 \times 10^{-4} \pm 9.21 \times 10^{-5}$	$8.39 \times 10^{-6} \pm 5.82 \times 10^{-5}$
D	$3.41 \times 10^{-4} \pm 7.66 \times 10^{-5}$	$2.91 \times 10^{-4} \pm 9.25 \times 10^{-5}$	$8.39 \times 10^{-6} \pm 5.82 \times 10^{-5}$
D/σ	4.44	3.15	0.14

Note. The measurements are given in pixel units, and the scale is $3\rlap{.}''98$ per pixel.

Table 4
Modeled Centroid Shifts Due to Transits on the Known Stars in the Aperture with Depths that Reproduce the Observed Depth

Object	Modeled D	D/σ	Object	Modeled D	D/σ	Object	Modeled D	D/σ
Kepler-9 b	1.22×10^{-3}	16.0	Kepler-9 c	1.10×10^{-3}	11.9	KOI-377.03	5.02×10^{-5}	0.86
Comp 1	depth > 1	...	Comp 1	depth > 1	...	Comp 1	1.45×10^{-4}	2.49
Comp 2	9.77×10^{-3}	127	Comp 2	8.75×10^{-3}	94.6	Comp 2	4.01×10^{-4}	6.89
Comp 3	depth > 1	...	Comp 3	depth > 1	...	Comp 3	5.33×10^{-4}	9.16
Comp 4	1.44×10^{-2}	188	Comp 4	1.29×10^{-2}	139	Comp 4	5.90×10^{-4}	10.1

Notes. Shifts are given in pixel units, and the scale is $3\rlap{.}''98$ per pixel. For Kepler-9 b and Kepler-9 c transits on some companions can be ruled out because they require depth > 1.

the primary, and corresponds to [Fe/H] = +0.12 and an age of 1 Gyr. The secondary and tertiary masses were allowed to vary freely between 0.10 $M_\odot$ (the lower limit in the models; see footnote 22) and 1.40 $M_\odot$, as mentioned earlier, seeking the best fit to the photometry. The inclination angle was also free, and the orbits were assumed to be circular. In both Kepler-9 b and c, which have similar transit signals, we find that the best-fitting hierarchical triple blend model corresponds to secondaries that are approximately 1.0 and 0.5 mag fainter than the primary, respectively, and tertiaries that are at the lower limit of the isochrone range (late M dwarfs). However, these fits give a poor match to the photometry: BLENDER is unable to simultaneously reproduce the total duration of the transit and the central depth, given the constraints on the brightness and size of the stars from the isochrones. This type of blend scenario is therefore clearly ruled out. We illustrate this for Kepler-9 b in Figure 4, where the best-fit planet model is also shown for reference. Much better matches to the data can be found if additional light from a fourth star along the line of sight is incorporated into the model, providing extra dilution. We find that this fourth star is required to be nearly as bright as the primary, and the optimal model changes in such a way that the secondary also becomes as bright as the primary (so that its size enables the duration of the transits to be reproduced), while the tertiary remains a small star. This rather contrived scenario requiring two bright stars that are nearly identical to the main star would be easily recognized in our high-resolution imaging for separations larger than about $0\rlap{.}''1$ (see, e.g., Figure 2), in our centroid analysis for separations larger than $0\rlap{.}''06$, or would otherwise produce obvious spectroscopic signatures unless all three bright objects happened to have the same radial velocity.

We next considered blends involving eclipsing binaries in the background, by removing the constraint on the distance. In this case a solar-metallicity isochrone was adopted for the binary, with a representative age for the field of 3 Gyr. We explored a wide range of relative distances, and we first considered main-sequence stars only, again with circular binary orbits. The results for Kepler-9 b and c are once again similar to each other, and we illustrate them for Kepler-9 c in Figure 5. The axes correspond to the distance modulus difference $\Delta\delta$ as a function of the tertiary mass. Contours represent constant differences in the χ^2 of the
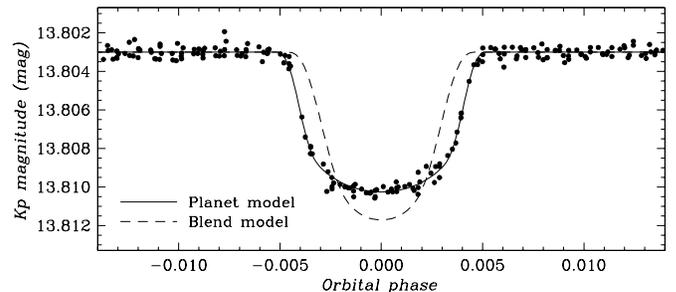

Figure 4. Light curve of Kepler-9 b ($P = 19.24$ days) with the best-fit blend model for the case of a hierarchical triple (candidate + physically associated eclipsing binary). The best-fit planet model is shown for reference. The poor fit of the blend model rules out this configuration.

fit compared to the best-fit planet model and are labeled in units of the statistical significance of the difference (σ). We draw two main results from this figure. One is that the light curve fits strongly prefer the smallest available tertiary masses from the isochrones (0.10 $M_\odot$), and would in fact yield better fits for even smaller tertiaries (i.e., planets). Additionally, the best solutions cluster toward equal distances for the binary and the primary star, effectively converging toward the equivalent of the hierarchical triple scenario considered earlier. No acceptable solutions exist with the binary at a significant distance behind the primary star. The best fit to the light curve of Kepler-9 c is similar to the one shown in Figure 4 (dashed curve), which is not particularly good. The $\Delta\delta$ versus tertiary mass diagram for Kepler-9 b is qualitatively the same. Allowing the secondary to be a giant star gives a very poor fit to the photometry: the duration of the transit is very much longer than observed, there is out-of-eclipse modulation due to distortions in the giant, and all solutions place the binary at an implausibly large distance. We conclude that blend configurations involving background eclipsing binaries in which the tertiary is a star are not a viable explanation for either of these two signals.

We then explored background eclipsing binaries in which the tertiaries are planets rather than stars. This allows their radii to be smaller, possibly providing a better fit to the *Kepler* photometry. The orbits were considered to be circular, as before.
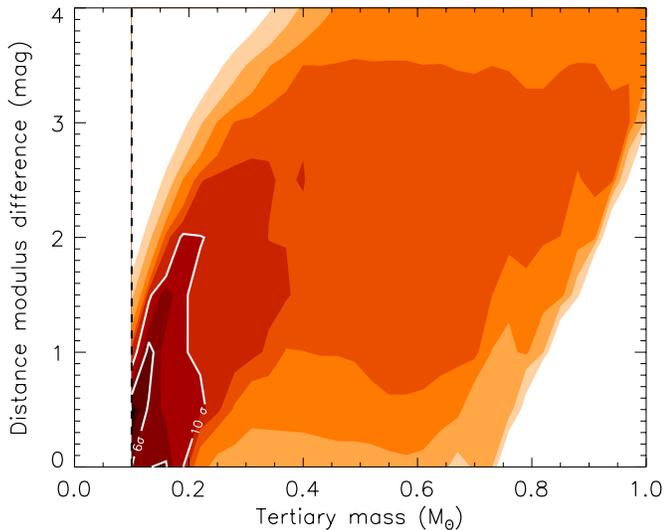
Figure 5. Map of the χ^2 surface (goodness of fit) corresponding to a grid of blend models for Kepler-9 c ($P = 38.91$ days) involving background eclipsing binaries with circular orbits. The separation between the binary and the primary is expressed in terms of the distance modulus difference. Contours are labeled with the χ^2 difference from the best planet model fit (expressed in units of the significance level of the difference, σ) and are plotted here as a function of the mass of the tertiary star. The dashed line at 0.1 $M_\odot$ indicates the lower limit to the tertiary mass set by the model isochrones we use.

(A color version of this figure is available in the online journal.)

Figure 6. Map of the χ^2 surface corresponding to a grid of blend models for Kepler-9 c involving background eclipsing systems in which the tertiary is a (dark) planet, in a circular orbit around the secondary. Contours are labeled with the χ^2 difference from the best-planet model fit (expressed in units of the significance level of the difference, σ). Two dashed lines of equal magnitude difference (ΔKp) are indicated and show that all viable blend fits (with confidence level $< 3\sigma$) have secondaries that are bright enough to have been detected spectroscopically ($\Delta Kp < 2$).

(A color version of this figure is available in the online journal.)

Figure 6 shows the results for Kepler-9 c, this time in the plane of separation versus secondary mass. Once again the fits tend to favor an equal distance for the binary and the primary star, and background scenarios with the binary far behind provide unacceptably poor matches to the light curve. A second noteworthy result is that these solutions have a strong preference for secondary stars that are quite similar to the primary. All acceptable fits to the light curve correspond to relatively bright secondaries with $\Delta Kp < 1.5$ mag (see Figure 6). The best of these solutions is of about the same quality as a planet model and has a secondary of mass 0.98 $M_\odot$ that is only 100 K cooler and 0.3 mag fainter than the primary in the *Kepler* band. This somewhat artificial case of "twin" stars is a result we have seen often in simulations for other *Kepler* candidates. The tertiary in this type of blend solution comes out about $\sqrt{2}$ larger than in a planet model because the transit is diluted by another star of approximately equal size and brightness. One may debate whether this situation should actually be referred to as a "false positive" for Kepler-9, since the signal would still correspond to a gas giant planet, only that this planet would be $\sqrt{2}$ larger, and it would be orbiting a different star. Alternatively, it could be thought of simply as an overlooked dilution factor in a true planetary system. In any event, the lack of evidence for this bright twin star in the spectroscopy or in our high-resolution imaging or centroid analysis for Kepler-9 does not support this scenario.

As a particular case of this family of configurations, we examined blends in which the star–planet pair is constrained to be at the same distance as the primary, i.e., effectively in a hierarchical system. The secondary properties were therefore taken from the same isochrone as the primary, and the orbits were assumed to be circular. An excellent fit to the light curve is possible for a tertiary that is about $\sqrt{2}$ larger than in a true planet model, but not surprisingly, we find once more that the secondary must be as bright as the primary.
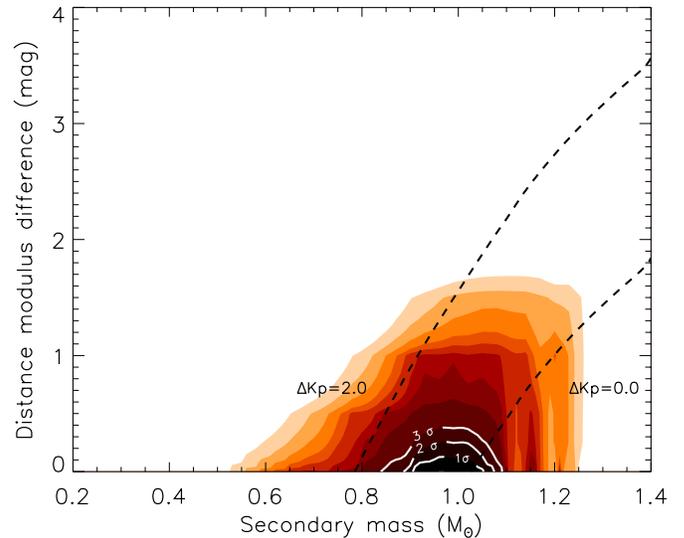
Additional tests were run to examine the impact of changing the age adopted for the isochrone of the secondary in a background star–planet pair or the addition of light from a fourth object in the aperture. In the first case, changing the age from 3 Gyr to 1 Gyr produced a small shift of the contours in Figure 6 downward and to the right that is simply due to the change in intrinsic brightness of the secondary star, and does not alter our conclusions. Adding "fourth light" further attenuates the eclipses of the star–planet pair. To compensate, BLENDER requires a slightly deeper eclipse, and in order to preserve the shape of the signal (total duration, and slope of ingress/egress), this is achieved by bringing the secondary closer to the primary. As a result, for relatively bright fourth light the contours are shifted downward by approximately the difference in magnitude between the primary and the fourth star, again without changing the conclusions.

One may also imagine blend scenarios in which the eclipsing binary is in the foreground, rather than the background. We explored this possibility by extending the simulations to negative values of $\Delta\delta$. As before, we adopted circular orbits and a 3 Gyr isochrone for the foreground system. Binaries with stellar tertiaries are clearly ruled out as they yield fits to the light curve that do not match its shape, and additionally they predict a fairly obvious secondary eclipse that is not seen in the data. We focus therefore on blends in which the tertiary is a planet, and we illustrate the results for Kepler-9 c. In this case we find there are many acceptable solutions with χ^2 values differing from the best-planet fit at the level of 1σ or less. These solutions span a range of secondary masses and a range of foreground separations, implying a wide range not only in apparent brightness for the secondary, but also in color. Models in which the secondaries are brighter than the primary and of significantly different spectral type would be inconsistent with the spectroscopic parameters derived for Kepler-9, and are excluded. Plausible solutions remain, in principle, for fainter
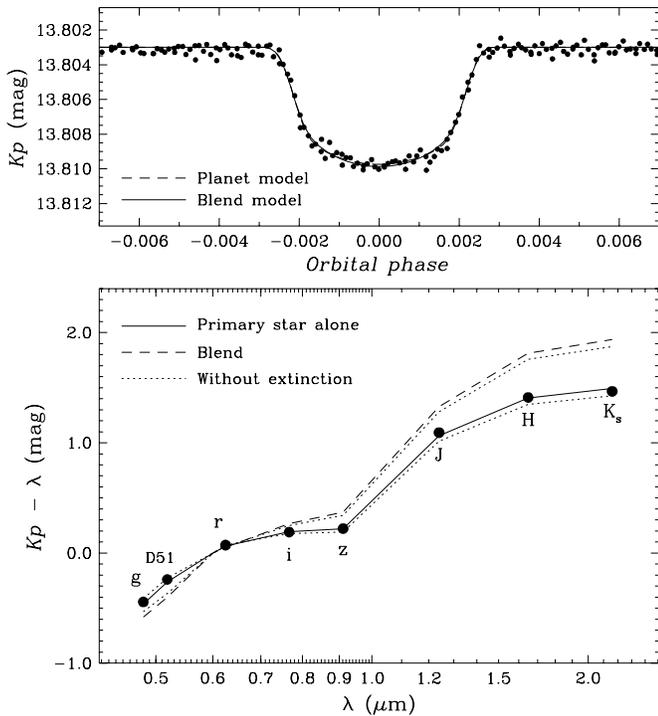
Figure 7. Top: light curve of Kepler-9 c with the best-fit blend model for the case of contamination by a foreground eclipsing pair with a circular orbit in which the tertiary is a planet. The pair consists of an M2 dwarf (0.56 $M_\odot$, 0.58 $R_\odot$) and a 0.91 R_{Jup} companion 450 pc in front of the primary, which is at 750 pc. This fit is statistically indistinguishable from best-fit planet model, also shown for reference. Bottom: measured colors for Kepler-9 (dots) compared with the predictions from the blend model in the top panel. A small amount of extinction (0.15 mag kpc^{-1}) has been included in these predictions. The results without considering extinction differ little and are shown with dotted lines. The color measurements clearly rule out such a blend.

Figure 8. Effect of eccentricity on the duration of transits relative to the circular orbit case (Δ/Δ_{circ}), on the impact parameter (b/b_{circ}), and on the displacement ($\phi_{sec} - 0.5$) of the secondary eclipses relative to phase 0.5, all shown as a function of the longitude of periastron ω. The different curves correspond to eccentricities from 0.1 to 0.7 in steps of 0.1.

foreground secondaries, which necessarily involve later-type stars. We find that of these, the only ones that yield acceptably good fits to the *Kepler* photometry, with χ^2 values differing from the planet fit by less than 3σ, correspond to secondaries that are within about 1.5 mag of the primary in brightness, and are of course redder. These would be valid blend configurations so long as the secondaries are close enough to the primary to be spatially unresolved (angular separations $\lesssim 0\farcs1$), and at the same time faint enough to have gone undetected in the spectra. Stars that are within ~2–2.5 mag of the primary would generally have been seen spectroscopically, as indicated in Section 3.2, and this would exclude these remaining foreground blend configurations. Nevertheless, to be conservative, let us assume for the moment that a star 1.5 mag fainter than the primary has still managed to elude detection in our spectra. This corresponds to the faintest secondary in a foreground blend scenario that still allows for a satisfactory fit to the light curve, and would be the most difficult case of this kind to disprove. This fit is shown in the top panel of Figure 7 and is statistically indistinguishable from a planet model fit. The secondary in this configuration is an M2 dwarf ($M = 0.56\ M_\odot$) 1.53 mag fainter than the primary, eclipsed by a 0.91 R_{Jup} planetary companion, and is located at a distance of 300 pc. The primary in this scenario is at 750 pc.

Other properties of this particular blend such as magnitudes and colors can be computed easily with BLENDER, and compared with observations. Apparent magnitudes for Kepler-9 are available from the KIC for a variety of passbands including Sloan
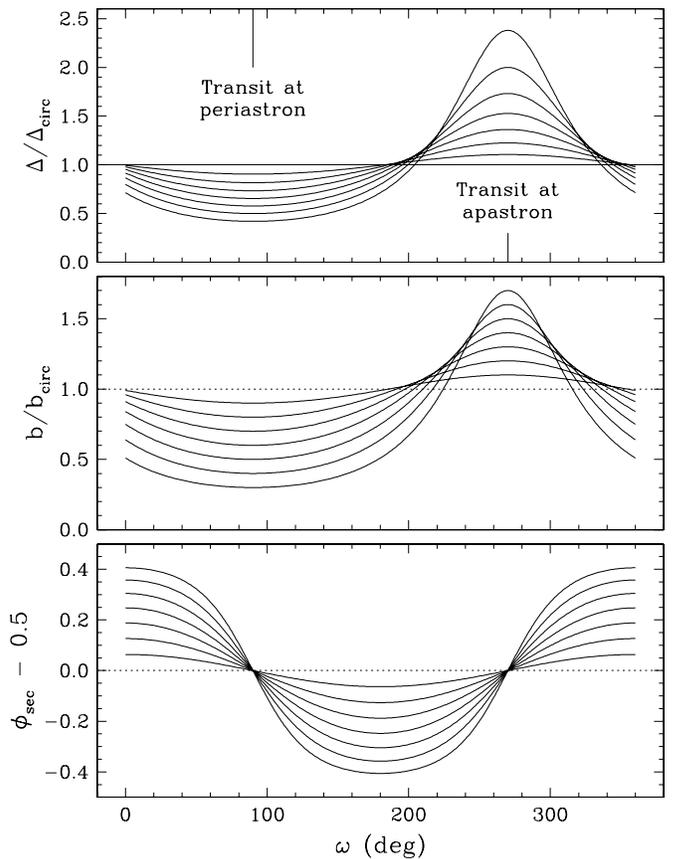
$griz$, a special-purpose passband referred to as D51 (centered on the Mg I b triplet at 518.7 nm), and JHK_s from the 2MASS catalog. The lower panel of Figure 7 shows various color indices ($Kp - \lambda$) predicted by BLENDER both for the primary star alone and for the blend. Those of the primary are well reproduced by the model, and we find that a small amount of interstellar extinction leads to an even better match (solid line in the figure). The colors of the blend, on the other hand, disagree with the measured colors and deviate by more than 0.4 mag for the reddest index, $Kp - K_s$. We are therefore able to exclude, solely on the basis of its color, this most difficult of the scenarios involving foreground star–planet pairs that could mimic the 19 day and 39 day signals in the light curve of Kepler-9. Larger-mass secondaries would not be as red and still allow for good fits to the photometry, but they are intrinsically brighter and would be recognized more easily.

The above simulations have all assumed circular orbits for the blended eclipsing binaries or star–planet pairs, which is not necessarily realistic given the relatively long periods of Kepler-9 b and c. Eccentricity affects the speed of the secondary and tertiary in their relative orbit, and therefore can change the duration of the transit, making it shorter or longer than in a circular orbit, depending on the orientation (longitude of periastron, ω). It also changes the impact parameter, all else being equal. And finally, it shifts the location of the secondary eclipse. The magnitude of these effects is illustrated in Figure 8 for eccentricities between 0.1 and 0.7. The most important effect for our purposes is on the transit duration. Given
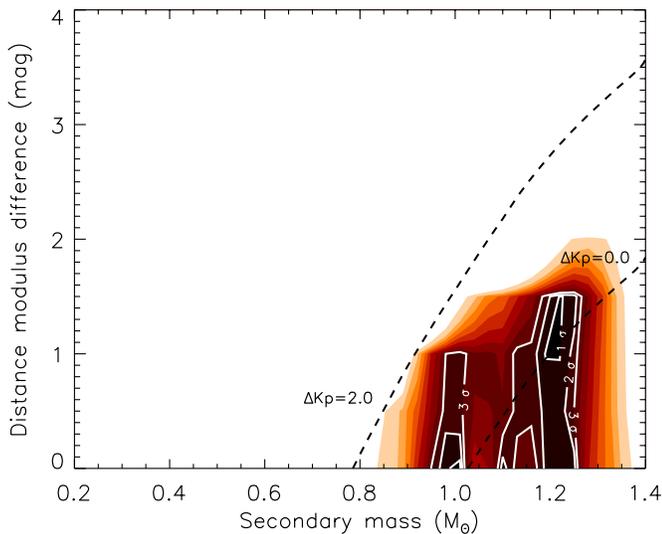
Figure 9. Same as Figure 6 (Kepler-9 c), restricted to star–planet orbits having $e = 0.3$ (concentration of contours on the left) and 0.5 (right), and $\omega = 90°$. This orientation corresponds to transits that occur at periastron. Comparison with Figure 6 shows that these solutions allow for more massive (larger) secondary stars than in the case of circular orbits, but the brightness of these blends is still within 2 mag of the target, and is ruled out by spectroscopy.

(A color version of this figure is available in the online journal.)

a fixed (measured) duration, eccentric orbits may allow blends with smaller or larger secondary stars than in the circular case to still provide satisfactory fits to the light curve, effectively increasing the pool of potential false positives. The limiting cases correspond to $\omega = 90°$ and $270°$, in which the line of apsides is aligned with the line of sight and the transit occurs at periastron (accommodating larger secondaries) or apastron (smaller secondaries), respectively. Extensive simulations for these two extreme situations show that allowing for eccentric orbits does not change our conclusions regarding hierarchical triple systems, background eclipsing binaries, or background star–planet scenarios. We show this for the latter blend category in Figure 9, illustrated for the case of orbits with eccentricities of 0.3 and 0.5, and $\omega = 90°$. Comparison with Figure 6 indicates that in both cases the blends are still bright enough that we would have seen signatures of them in the spectra of Kepler-9. Larger eccentricities of $e = 0.7$ result in secondaries that are brighter still. For eccentric orbits oriented such that transits take place at apastron ($\omega = 270°$), we only find acceptable fits to the light curves for eclipsing star–planet pairs that are in the foreground (and involve smaller stars). However, as was the case for circular orbits, those blends are either too bright, too red, or both, and are thus also excluded.

The above, fairly exhaustive exploration of parameter space with BLENDER allows us to conclude that no configuration involving an eclipsing binary (or an eclipsing star–planet pair), either in the foreground or in the background, is able to provide a reasonable explanation for the signals of Kepler-9 b and c (see Table 5 for a summary of the configurations tested and the results). Many scenarios lead to light curves that match the detailed shape of the transit events, but none are simultaneously consistent with all of the other observational constraints. This includes spectroscopy, high-resolution imaging, centroid measurements, and photometry (colors). Therefore, even ignoring the evidence from TTVs, these results fully support the planetary nature of these objects and demonstrate the usefulness of BLENDER for validating transiting planet candidates from *Kepler*.

3.5. BLENDER *Analysis of KOI-377.03*

We proceed next to examine false positive scenarios for the shallowest signal in Kepler-9, with $P = 1.59$ days, which would correspond to a super-Earth-size planet. Because the period is so short in this case, and tidal forces in such binary systems have likely circularized the orbit (see, e.g., Mazeh 2008 and references therein), we do not consider non-zero eccentricities. Additionally, blends in which the secondary star is a giant need not be considered, as those cases are obviously ruled out because of the short orbital period and small implied semimajor axis of the orbit.

As for the larger signals considered above, hierarchical triple systems in which the tertiary is a star fail to provide good fits to KOI-377.03. A good match to the *Kepler* photometry can be found when the tertiary is allowed to be a much smaller object (i.e., a planet), but as was the case earlier, it requires a secondary that is very similar to the primary in brightness. The resulting size of the eclipsing object is $\sqrt{2}$ larger than in a planet model or slightly over $2\,R_\oplus$. This type of configuration was ruled out earlier based on the high-resolution imaging and the spectroscopy. Small tertiaries with appreciable mass, such as white dwarfs, induce tidal distortions on the primary due to the short orbital period that lead to significant out-of-eclipse variations in the light curve (ellipsoidal variability). These modulations are not seen in the photometry for Kepler-9, and such false positives are therefore also excluded.

Blends with an eclipsing binary in the background (the tertiary being a star) are able to reproduce the light curve just as well as a planet model. In Figure 10, we illustrate those results by showing the area of allowed parameter space in a diagram of distance modulus difference as a function of secondary mass. Acceptable fits with χ^2 differing from the planet model by less than 3σ are possible over a wide range of relative separations ($4.5 \leqslant \Delta\delta \leqslant 9$), but the secondaries are restricted to a relatively narrow interval in mass centered on the mass of the primary. These eclipsing binaries are all very distant and faint ($Kp \approx 19$–22) and have no effect on the colors of the blend. The more distant scenarios place the binary at implausibly large distances of up to 42 kpc (more than 10 kpc above the Galactic plane). The nearest configuration ($\Delta\delta = 4.5$; see Figure 10) has the binary at a distance of 5.3 kpc, and the primary at $\sim$670 pc. The secondary in this model is a late G star 5.5 mag fainter than the primary in the *Kepler* passband, eclipsed by a late M dwarf that produces no detectable secondary eclipse. The predicted brightness of this binary precisely matches that of the closest companion identified in the AO images (Comp 1, Table 1), located 2$.\!''$85 NE of the target. However, this and all wider visual companions are already ruled out at more than the 3σ confidence level by the lack of centroid motion, which would have revealed any blended eclipsing binaries at angular separations larger than about 0$.\!''$74 (Section 3.3). Even without this constraint from astrometry, the predicted $J-K_s$ color of the secondary in this blend is considerably redder than measured for this close AO companion, which would also disqualify it. Eclipsing binaries that are between 5 and $\sim$8.5 mag fainter than the main star provide acceptably good fits to the light curve (see Figure 10), and if they were angularly closer than 0$.\!''$74 from the target they may not be detectable in our AO or speckle observations, in our centroid motion analysis, nor in our spectra. They remain viable blend configurations, and would necessarily be at distances greater than 5 or 6 kpc. An example is shown in Figure 11, to illustrate that the fit is indistinguishable from a planet fit.

Table 5
Summary of Blend Configurations Tested for Kepler-9 b and c

False Positive Configuration[a]	Result	Blends Ruled Out
Hierarchical triple with stellar tertiary, MS		
Circular and eccentric orbits	Poor fits/sec. ecl.	Yes
Added fourth light	Twin star	Yes (imaging/spec./centr.)
Hierarchical triple with planetary tertiary, MS		
Circular and eccentric orbits	Twin star	Yes (imaging/spec./centr.)
Background EB with stellar tertiary		
Circular and eccentric orbits, MS and giants	Poor fits	Yes
Background EB with planetary tertiary, MS		
Circular and eccentric orbits	Twin star	Yes (imaging/spec./centr.)
1 Gyr isochrone for secondary	Little change	Yes (imaging/spec./centr.)
Added fourth light	Little change	Yes (imaging/spec./centr.)
Foreground EB with stellar tertiary, MS		
Circular and eccentric orbits	Poor fits/sec. ecl.	Yes
Foreground EB with planetary tertiary, MS		
Circular and eccentric orbits	Too bright/Too red	Yes (imaging/spec./centr./color)

Note.

[a] 3 Gyr isochrone and solar metallicity assumed for background and foreground stars, unless otherwise indicated. Abbreviations: MS, main-sequence secondary; imaging/spec./centr., high-resolution imaging, spectroscopy, and centroid analysis; sec.ecl., secondary eclipses predicted but not observed; EB, eclipsing binary.
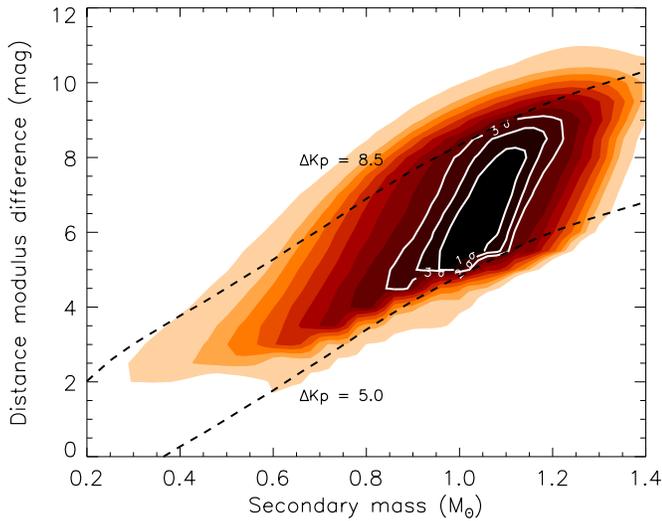

Figure 10. Map of the χ^2 surface for KOI-377.03 corresponding to a grid of blend models involving background eclipsing binaries with stellar tertiaries. Contours are labeled with the χ^2 difference from the best planet model fit (expressed in units of the significance level of the difference, σ). The dashed lines indicate levels of equal apparent magnitude difference ΔKp between the background binary and the primary star.

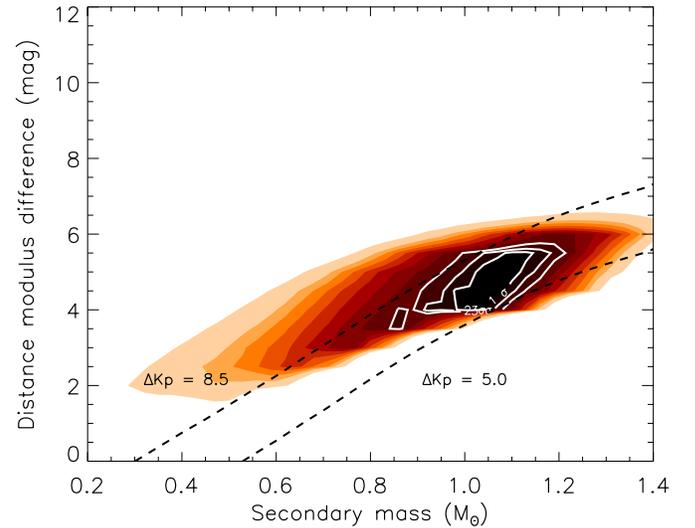(A color version of this figure is available in the online journal.)

Figure 12. Same as Figure 10, including the effect of differential extinction in the amount of 0.5 mag kpc^{-1}. The net effect of extinction is to compress and shift the contours toward smaller relative distances. The dashed lines indicate levels of equal apparent magnitude difference ΔKp between the background binary and the primary star and are the same as shown in Figure 10.

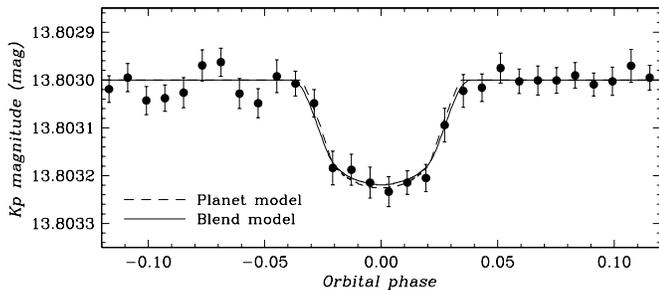(A color version of this figure is available in the online journal.)

Figure 11. Example of a blend model fit to KOI-377.03 involving a background eclipsing binary with a stellar tertiary (solid line). The secondary is similar in spectral type to the primary and 5.2 mag dimmer, and the tertiary is a late M dwarf. The eclipsing pair is 6 kpc behind the primary. This fit is statistically indistinguishable from the best-fit planet model, which is shown with a dashed line. The *Kepler* observations have been binned for clarity.

In the above calculations we have ignored interstellar extinction. However, given the large distances for the binaries in some of these blend configurations, it is worth exploring the effect of dust more carefully, which we have done by repeating the BLENDER simulations using a representative differential extinction coefficient of 0.5 mag kpc^{-1}. The results are shown in Figure 12 and indicate that the blend scenarios providing good fits to the *Kepler* photometry of KOI-377.03 are systematically shifted to smaller distances compared to the previous calculations. Their apparent brightness, however, changes relatively little, as can be seen by comparing the lines of equal ΔKp with those in Figure 10. Therefore, the overall impact of differential extinction on the permitted area of parameter space in terms of observable parameters is not as significant as might have appeared.
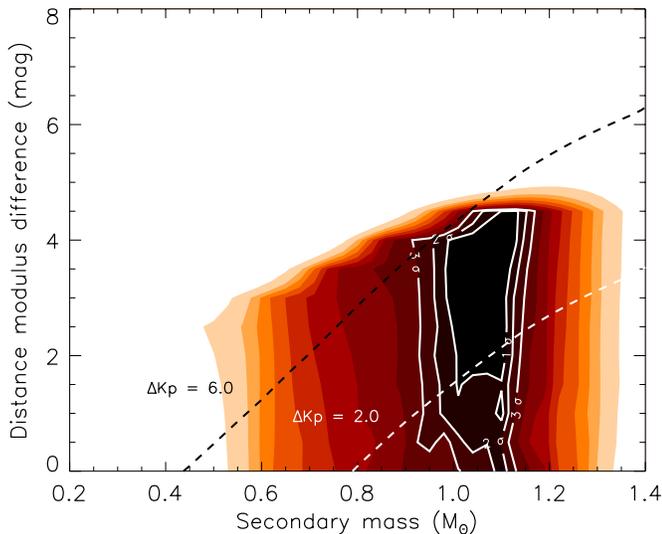
Figure 13. Same as Figure 12, but for the case in which the tertiary is a planet instead of a star. Differential extinction is included. Kinks in the contours are an artifact of the discreteness of our grid. The dashed lines indicate levels of equal apparent magnitude difference ΔKp between the background secondary and the primary star. The lower of these lines represents the constraint from the spectroscopy for Kepler-9 (see the text).

(A color version of this figure is available in the online journal.)

Figure 14. Same as Figure 13, shown here as a function of the tertiary radius. Kinks in the contours and closed inner contours for the 1σ and 2σ levels are an artifact of the discreteness of our grid. We indicate with a dashed line the lower limit for the size of the tertiaries that is set by the spectroscopic constraint on presence of bright stellar companions (see the text). The sizes of the Earth, Neptune, and Saturn are also indicated for reference.

(A color version of this figure is available in the online journal.)

Allowing the tertiary to be a smaller object such as a planet opens up a different area of parameter space for permissible background blends (Figure 13). When including extinction as before, acceptable fits to the light curve are possible for $\Delta\delta$ values from zero up to about 4.5. This upper limit corresponds to distances for the star–planet pair of about 4.8 kpc (with $\Delta Kp \approx 6$, or apparent magnitudes of $Kp \approx 20$) and is set by the maximum size of 1.8 $R_{\rm Jup}$ we have allowed for a planet. As in the configurations described before, the solutions constrain the secondary masses to be near that of the primary in order to match the detailed shape and observed duration of the transits, with a range from about 0.9 $M_\odot$ to 1.2 $M_\odot$. Therefore, the color of the blend is not as useful a discriminant in this case. Secondaries that are less than about 2 mag fainter than the primary would have been seen spectroscopically. This excludes a good fraction of the space of parameters, as indicated by the lower dashed line in Figure 13. Of the remaining blends of this kind between $\Delta Kp = 2$ and $\Delta Kp = 6$, only the ones with angular separations smaller than about 1″ are allowed by the constraints from our AO imaging (see Figure 2), but the centroid analysis is even more restrictive and rules out stars outside of 0″.74. At closer separations, the high-resolution images rule out all blends that are brighter than the sensitivity limit indicated in Figure 2 (i.e., those that fall above the curves).

As expected from the fixed duration and depth of the transit-like signal of KOI-377.03, the size of the tertiary in these configurations correlates with the secondary mass. Due to this correlation, small tertiaries with $R \lesssim 0.3\,R_{\rm Jup}$ (roughly Neptune-size and smaller) are further excluded because the eclipses they produce are already very shallow, and further dilution by the primary would make them too shallow to fit the photometry. In order to avoid this, the secondaries in those blends must be relatively small late-G type stars that are nearby, and would therefore be bright enough ($\Delta Kp \lesssim 2$) that they would have been detected in our spectra as a second set of lines. Thus, BLENDER effectively places limits not only on the secondary, but also on the size of the tertiary (see Figure 14).
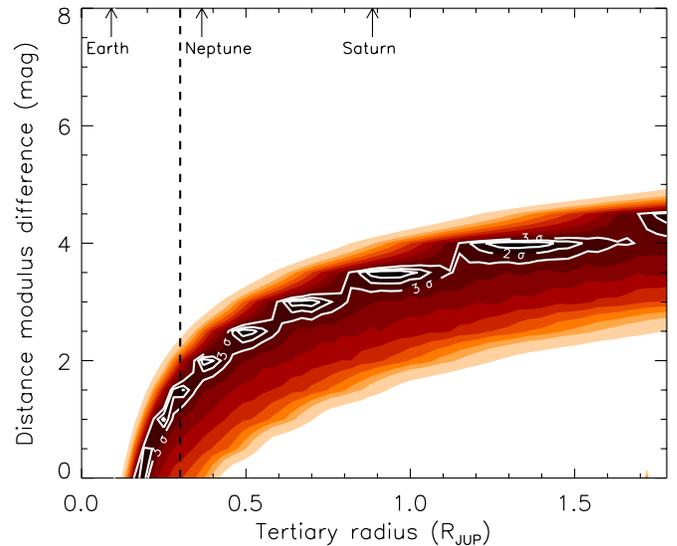
In particular, blends with a white dwarf eclipsing a background star are also ruled out for the same reason described above. Additionally, the predicted light curves for such cases with white dwarf tertiaries show ellipsoidal variability, which is not observed.[26] Many of the larger tertiaries correspond to gas giants (Saturn-size or larger), which implies a qualitative difference in their nature compared to the alternate model of a true Earth- or super-Earth-size planet. In this sense these blends may properly be considered "false positives," as opposed to the configurations discussed earlier requiring twin stars, which only change the tertiary radius by $\sqrt{2}$.

Finally, we examine the possibility that the true period of the KOI-377.03 signal is twice the nominal value. Alternating events would then correspond to the primary and secondary eclipses of a blended eclipsing binary (the tertiary being a star in this case), which may in general be of different depth. In KOI-377.03 there is no compelling evidence for a depth difference between odd- and even-numbered events, but this is difficult to establish in a faint star such as this for a signal that is only 0.2 mmag deep. The results of extensive simulations with BLENDER for this scenario are illustrated in Figure 15. The best fits correspond to blended binaries far in the background, and do not indicate a significant difference in depth between the primary and secondary eclipses. However, these fits provide only a poor representation of the *Kepler* light curve, and can therefore be confidently ruled out. This is seen in Figure 16. The top panel shows the closest fit to the full light curve together with the data, and in the bottom panel we have binned the measurements to facilitate the comparison. This solution involves an eclipsing

---

[26] We note, for completeness, that the mass of a white dwarf would generally also be sufficient to induce tidal synchronization in the secondary star, resulting in line broadening that could in principle render it more difficult to detect in the spectrum. However, given the orbital period and typical secondary sizes allowed by BLENDER, we estimate the rotational broadening to be no more than $\sim$30 km s^{-1}, which should still allow that star to be seen spectroscopically if it were bright enough. In any case, white dwarfs are excluded as viable tertiaries for the reasons mentioned in the text.
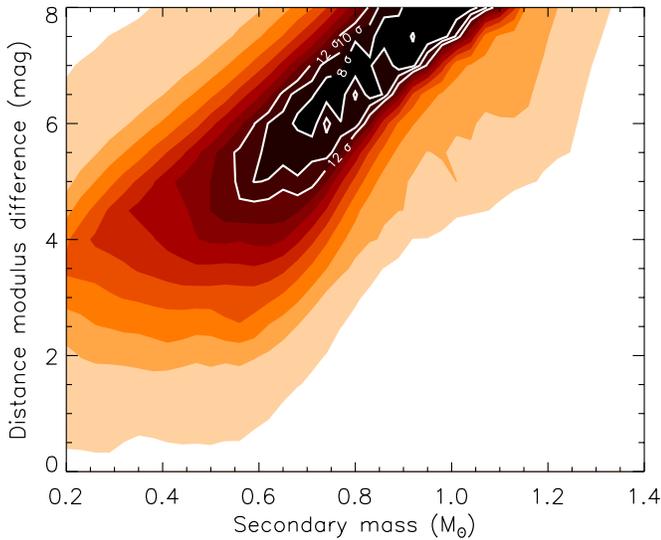
Figure 15. Same as Figure 10, but for the case in which the orbital period is assumed to be twice the nominal value ($2P = 3.185702$ days).

(A color version of this figure is available in the online journal.)

Figure 16. Blend model of a background eclipsing binary with twice the nominal period of KOI-377.03. Top: *Kepler* observations and best blend fit corresponding to two nearly equal mid G dwarfs eclipsing each other, and located 20.4 kpc behind the primary. Bottom: binned observations compared against the blend model in the top panel. The fit corresponding to a planet model is shown for reference.

pair of mid-G dwarfs at 21 kpc and 7.2 mag fainter than the primary, and the fit is visibly worse than that corresponding to a planet at half the period, which is shown with the dashed line.

In summary, the BLENDER analysis of this section coupled with constraints from spectroscopy, high-resolution imaging, and centroid motion measurements rules out a large fraction of the false positives that could produce the 1.59 day signal, but not all (see Table 6). The remaining configurations involve main-sequence background stars that are similar to the primary in spectral type (late F to early K, or about $0.9 \, M_\odot$ to about $1.2 \, M_\odot$) and are eclipsed either by another smaller main-sequence star or by a planet with $R_p > 0.3 \, R_{\rm Jup}$ (Neptune-size or larger). These blends range in apparent brightness from $Kp \approx 19$ to $Kp \approx 22$ for stellar tertiaries, and from $Kp \approx 16$ to $Kp \approx 20$ if the tertiaries are planets, and must be closer than $0\rlap{.}''74$ from the target. At separations under $0\rlap{.}''74$ our imaging observations allow us to rule out the brighter of these blends, and only the ones with Δm below the sensitivity curves in Figure 2 would remain undetected.

3.6. Likelihood of Remaining Blend Scenarios for KOI-377.03

In the previous section, we have considered a wide variety of possible blend scenarios for KOI-377.03 involving secondaries of different spectral types (main-sequence stars and giants), eclipsing objects of both planetary and stellar nature (including white dwarfs), and configurations consisting of chance alignments with a foreground or background contaminant, as well as hierarchical triple systems. While these represent the most common and obvious configurations one can imagine, in principle there could also be more contrived scenarios that we have not thought of. These should be intrinsically much less likely, a priori, but can nevertheless not be completely ruled out. Therefore, we proceed below on the assumption that any such situations we have not considered have a small rate of occurrence, at least compared to the ones we have discussed explicitly.

In order to provide the basis for an estimate of the confidence level for the planetary status of KOI-377.03, we describe here the calculation of the likelihood that the signal is due to a background blend involving either a stellar tertiary or a planetary tertiary, taking into account the constraints on brightness and
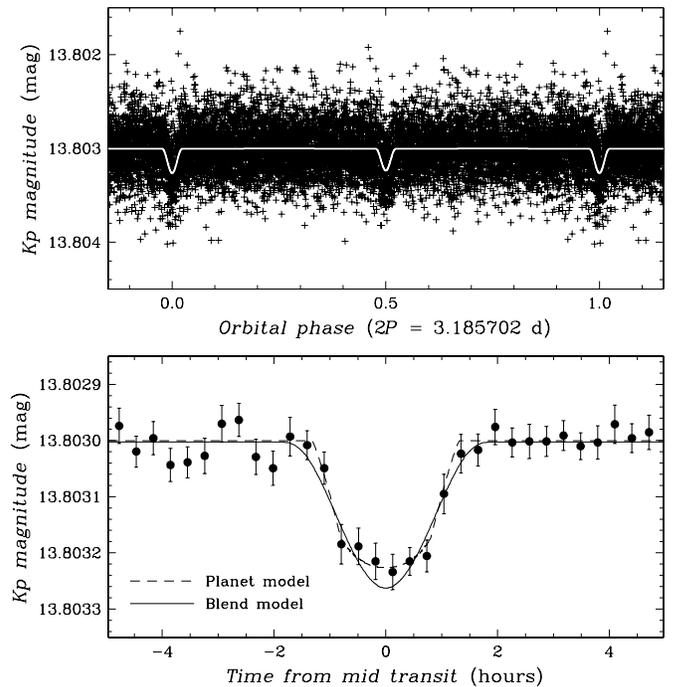
other properties indicated in the previous section. Because this type of calculation is likely to be relevant for other *Kepler* candidates, we describe it here in some detail.

The frequency of stars in the mass range permitted by BLENDER was estimated using the Besançon Galactic structure models of Robin et al. (2003), specifically for the *R* band, which is the closest available to the *Kepler* passband. We used an aperture of 1 square degree centered on Kepler-9, and we performed the stellar density calculations in half-magnitude bins of apparent brightness, accounting for interstellar extinction as we did in the BLENDER simulations, with a coefficient of 0.5 mag kpc^{-1} in *V*. The range of allowed secondary masses for each magnitude bin was taken directly from Figure 12 for blends with stellar tertiaries, and from Figure 13 for blends with planetary tertiaries.

Using the density of stars in each magnitude bin, we calculated the fraction that would remain undetected after our high-resolution imaging (speckle and AO observations), spectroscopy, and centroid motion analyses. The results are listed in Table 7. The first two columns give the Kp magnitude range of each bin and the magnitude difference ΔKp compared to the target, calculated at the upper edge of the magnitude bins. For convenience the calculations for blends with stellar tertiaries and planetary tertiaries are listed separately. For the stellar tertiary case, Column 3 reports the density of stars obtained from the Besançon models, restricted to the mass range allowed by BLENDER as shown in Figure 12. Column 4 lists the maximum angular separation $\rho_{\rm max}$ at which stars in the corresponding magnitude bin would go undetected in our imaging observations, read off from Figure 2, and taken at the center of each magnitude bin. Centroid motion analysis rules out eclipsing binaries beyond $0\rlap{.}''74$, so $\rho_{\rm max}$ is constant at that value for the last few bins in which this provides a stronger constraint than the

Table 6
Summary of Blend Configurations Tested for KOI-377.03

False positive configuration[a]	Result	Blends ruled out
Hierarchical triple with stellar tertiary, MS	Poor fits	Yes
White dwarf tertiaries	Poor fits	Yes
Hierarchical triple with planetary tertiary, MS	Twin star	Yes (imaging/spec./centr.)
Background EB with stellar tertiary, MS		
With and without extinction	Good fits	Not all
Giant secondaries	P too short	Yes
White dwarf tertiaries	Poor fits	Yes
Twice the period	Poor fits/sec. ecl.	Yes
Background EB with planetary tertiary, MS		
Jupiters, Neptunes, super-Earths, with extinction	Good fits	super-Earths
Giant secondaries	P too short	Yes
White dwarfs, with extinction	Good fits	Yes (imaging/spec./centr.)
Foreground EB with stellar tertiary, MS	Poor fits	Yes
Foreground EB with planetary tertiary, MS	Poor fits	Yes

Note.

[a] 3 Gyr isochrone and solar metallicity assumed for background and foreground stars. Orbits are circular. Abbreviations: MS = main sequence secondary; imaging/spec./centr. = high-resolution imaging, spectroscopy, and centroid analysis; sec.ecl. = secondary eclipses predicted but not observed; EB = eclipsing binary.

Table 7
Blend Frequency Estimate for KOI-377.03 Based on Stellar Densities and Frequencies of Eclipsing Binaries and Transiting Planets

		Blends Involving Stellar Tertiaries				Blends Involving Planetary Tertiaries				
Kp Range (mag)	ΔKp (mag)	Stellar Density (per sq. deg)	ρ_{max} ('')	Stars (10^{-6})	EBs $f_{EB} = 0.53\%$ (10^{-6})	Stellar Density (per sq. deg)	ρ_{max} ('')	Stars (10^{-6})	Transiting Jupiters 6–15 $R_\oplus$, $f_{Jup} = 0.11\%$ (10^{-6})	Transiting Neptunes 3.4–6 $R_\oplus$, $f_{Nep} = 0.10\%$ (10^{-6})
(1)	(2)	(3)	(4)	(5)	(6)	(7)	(8)	(9)	(10)	(11)
13.8–14.3	0.5	...	...	...	...	...	...	...	...	...
14.3–14.8	1.0	...	...	...	...	...	...	...	...	...
14.8–15.3	1.5	...	...	...	...	...	...	...	...	...
15.3–15.8	2.0	...	...	...	...	...	...	...	...	...
15.8–16.3	2.5	...	...	...	...	563	0.14	2.675	0.0029	0.0027
16.3–16.8	3.0	...	...	...	...	595	0.17	4.168	0.0046	0.0042
16.8–17.3	3.5	...	...	...	...	588	0.20	5.701	0.0063	0.0057
17.3–17.8	4.0	...	...	...	...	430	0.23	5.514	0.0061	0.0055
17.8–18.3	4.5	...	...	...	...	292	0.25	4.424	0.0049	0.0044
18.3–18.8	5.0	2	0.35	0.059	0.0003	125	0.35	3.712	0.0041	0.0037
18.8–19.3	5.5	14	0.45	0.687	0.0036	57	0.45	2.798	0.0031	0.0028
19.3–19.8	6.0	14	0.55	1.027	0.0054	24	0.55	1.760	0.0019	0.0018
19.8–20.3	6.5	20	0.70	2.376	0.0126	...	...	...	...	...
20.3–20.8	7.0	13	0.74	1.726	0.0091	...	...	...	...	...
20.8–21.3	7.5	3	0.74	0.398	0.0021	...	...	...	...	...
21.3–21.8	8.0	4	0.74	0.531	0.0028	...	...	...	...	...
21.8–22.3	8.5	0	0.74	0.000	0.0000	...	...	...	...	...
22.3–22.8	9.0	0	0.74	0.000	0.0000	...	...	...	...	...
Totals		70	...	6.804	**0.0359**	2674	...	30.752	**0.0339**	**0.0308**
Blend frequency (BF) = $(0.0359 + 0.0339 + 0.0308) \times 10^{-6} = 1.006 \times 10^{-7}$										

Note. The total blend frequencies in Columns 6, 10, and 11, shown in bold font, are calculated as the sum of the individual frequencies in each magnitude bin.

imaging limits. The total number of stars of the appropriate mass range in a circle of radius ρ_{max} around Kepler-9 is then given for each bin in Column 5, in units of 10^{-6}. We note that the secondary mass and angular separation constraints together reduce the number of background stars to be considered as potential contaminants by a factor of 97,500 compared to the number that would otherwise be expected to fall within the photometric aperture of *Kepler*. This is already indicative of a significantly reduced chance of having a false positive.

The intrinsic frequency of eclipsing binaries in the field is a key ingredient in the calculation, and for this we have relied on the results of Prsa et al. (2011), which are based on

the *Kepler* observations themselves. These authors found the average occurrence rate of eclipsing binaries among the *Kepler* targets down to $Kp \approx 16$ to be approximately 1.2% across the entire field. This may be a slight overestimate because it counts as eclipsing binaries targets that are actually blended with a background binary that is not a target, though the effect is likely small. There is little information available on fainter eclipsing binaries, so we assume here that a similar frequency holds. More importantly, many of these eclipsing binaries cannot produce signals such as that of KOI-377.03 because their light curves have the wrong shape. Examples include contact binaries and ellipsoidal variables, in which the

brightness changes continuously throughout the cycle, rather than presenting sharp transit-like events such as we observe. Additionally, semi-detached systems would have eclipses that are too long and also of the wrong shape. We therefore exclude these from the tally. With this adjustment, the frequency of eclipsing binaries capable of producing blends with the right shape is 0.53%. Multiplying the star counts in Column 5 by this frequency, we obtain the total number of blends expected in each magnitude bin, which is reported in Column 6.

Columns 7–9 are similar to Columns 3–5, but for blends involving star–planet pairs. Note that the range of allowed magnitudes is different in this case, as is the range of secondary masses used to compute the densities in Column 7 (see Figure 13). Following the size ranges adopted by Borucki et al. (2011), we consider three categories of transiting planets as potential companions: super-Earths (1.25–2 $R_\oplus$), Neptune-size planets (2–6 $R_\oplus$), and Jupiter-size planets (6–22 $R_\oplus$ or equivalently $\sim$0.5–2.0 $R_{\rm Jup}$). Planetary tertiaries smaller than 0.3 $R_{\rm Jup}$ = 3.4 $R_\oplus$ are ruled out by BLENDER, as false positives with such tertiaries can only reproduce the light curve if the secondaries are relatively bright, and those would have been detected spectroscopically. This effectively eliminates all super-Earths, and a fraction of the Neptunes. For the intrinsic frequency of transiting planets we have relied on the results from the first 43 days of *Kepler* observations as reported by Borucki et al. (2011). That census is unlikely to have missed many Neptune- or Jupiter-size planets (except ones with very long periods), although it may include false positives, so we consider the count to be conservative for the purpose of computing blend frequencies. Those authors presented a list of 306 targets with at least one transiting planet candidate and described another 400 targets with one or more transit-like signals that have not yet been released. Of the 306 targets, 24% would correspond to Jupiter-size planets and 23% to Neptune-size planets. One may reasonably assume that the 400 sequestered targets contain a larger fraction of smaller Earth- or super-Earth-size planets (which cannot mimic the light curve of KOI-377.03; see Section 3.5), for at least two reasons. Smaller planets are the main focus of the *Kepler* Mission, and they require more intensive follow-up efforts for validation, which is why those targets have not yet been made public. Second, these 400 targets are brighter, which makes smaller planets around them easier to detect. Consequently, the assumption of similar Jupiter- and Neptune-size planet frequencies as given above, but for the entire sample of 306 + 400 targets showing transit-like features, is a conservative one. Scaling to the full sample of 156,097 *Kepler* targets (Borucki et al. 2011), we find an upper limit to the frequency of transiting Jupiter-size and Neptune-size planets of 0.11% and 0.10%, respectively.[27] With these adopted frequencies, the resulting numbers of blends involving these types of planets are listed in Columns 10 and 11 of Table 7.

The total blend frequencies (BFs) in each of Columns 6, 10, and 11 are calculated as the sum of the individual frequencies in each magnitude bin and are shown in bold font. The three columns are then combined in the bottom section of the table to yield an overall BF of $\sim$1.0 × 10^{-7}.

This very small frequency corresponds to the number of false positives we expect to find a priori for Kepler-9. However, we point out that this *does not* translate directly into a false alarm probability, or equivalently into a confidence level that the candidate is orbited by a true super-Earth-size planet, as that requires knowledge of the rate of occurrence of such planets. For a random candidate star in the field the rate of false positives relative to the rate of true planets (false alarm rate, FAR) can be written quite generally as FAR = $N_{\rm FP}/(N_{\rm FP} + N_p)$, where $N_{\rm FP}$ is the number of false positives and N_p is the number of planets in the sample. Thus, the larger the number of planets we expect, the smaller the FAR.

We consider Kepler-9 to be fairly representative of a typical target in the field in terms of its spectral type (solar), brightness, and background stellar density (a function of Galactic latitude). In that case, the total number of blends can be taken to be approximately the product of BF and the size of the sample or $N_{\rm FP} =$ BF × 156,097 = 0.016. The number of small planets expected in the sample is of course not known, and determining it is precisely one of the goals of the *Kepler* Mission.

If we accept a confidence level of 99.73% (3σ) as being sufficient for validation of a transiting planet candidate (corresponding to FAR = 2.7 × 10^{-3}), then the minimum number of super-Earth-size planets N_p required in order to be able to claim this level of confidence is 6. Even though N_p is unknown, it is possible to make educated guesses as to what the *minimum* value would be in several ways, drawing on both theoretical and observational considerations.

Ground-based Doppler surveys continue to push toward the detection of smaller and smaller planetary signals. Lovis et al. (2008) have reported preliminary results from a sample of some 400 FGK stars observed with the HARPS instrument on the ESO 3.6 m telescope (see also Mayor et al. 2009), suggesting that as many as $\sim$30% of the targets may be orbited by close-in super-Earth- and Neptune-mass companions (5–30 $M_\oplus$) with periods up to 50 days. The peak in the period distribution seems to be around 10 days. By making use of the CoRoTlux tool (Fressin et al. 2007, 2009) we simulated a sample of 156,097 stars in the *Kepler* field based on the Besançon models employed earlier, and used the results from Lovis et al. (2008) to assign planets at random to each star, with a log-normal distribution of periods centered at 10 days. Approximate planetary radii were inferred from the masses using the structure models of Valencia et al. (2007), by drawing masses at random and assigning radii over the full range of compositions allowed by these models. We then retained only those in the super-Earth category, with $R_p \leqslant 2 \, R_\oplus$. The number of these planets that undergo transits in the *Kepler* field is calculated to be $N_p \approx 200$. If we were to accept this estimate, the corresponding false alarm rate would be FAR = 8 × 10^{-5}.

A similar Doppler survey of 166 G and K stars with the HIRES instrument on the 10 m Keck I telescope (Howard et al. 2010) has provided additional insights into the rate of occurrence of small-mass planets. The results suggest that approximately 18% of solar-type stars harbor planets in the range of 3 to 30 $M_\oplus$ with periods under 50 days. A calculation analogous to that carried out above for the transit probabilities and conversion from planetary masses to planetary radii leads to an estimate of $N_p \approx 120$ for the *Kepler* field. If we adopted this lower estimate, the corresponding false alarm rate would be FAR = 1.3 × 10^{-4}.

---

[27] As a check we may compare the above frequency of transiting Jupiter-size planets against results from the statistical study by Fressin et al. (2009). These authors combined the findings of various radial-velocity searches and folded-in the detections of very short-period systems detected by ground-based transit surveys, which are typically less common in Doppler searches. They found that 0.074% of solar-type stars have a transiting Jupiter-size planet. Our upper limit of 0.11% is consistent with this, given the presumably higher completeness of *Kepler* and the fact that a fraction of the *Kepler* candidates that is yet to be determined may turn out to be false positives once the follow-up is completed.

Population synthesis studies such as those of Ida & Lin (2004) and Mordasini et al. (2009) based on the formation of planets by the core accretion process and subsequent migration have provided tentative predictions of the properties of planets, including distributions of their masses, periods, and other characteristics. These theoretical models seem to point to a sizable population of super-Earths that may be several times larger than the number of Neptune- or Jupiter-mass planets in those simulations. Scaled to the size of the *Kepler* sample, this would imply that there could be several hundred small transiting planets. However, the authors caution that those results should be considered with great care as some of the physical ingredients in these models are still very uncertain.

A further estimate may be obtained from the preliminary *Kepler* results as reported by Borucki et al. (2011). Among the 306 targets listed there showing one or more periodic transit-like signals, 27 fall in the category of super-Earths. While it is true that these candidates have not yet been followed up and validated, and may therefore include some fraction of false positives, additional super-Earth-size planets are to be expected in the list of 400 unreleased candidates, which could make N_p considerably larger. This is particularly true since the targets in the latter list are all brighter than those in the publicly available set, and therefore the proportion of small planets is likely to be higher because the transit events are easier to detect. Nevertheless, if we were to accept that N_p is as small as 27, then the corresponding false alarm rate would be FAR = 6×10^{-4}.

There are caveats associated with each of the observational estimates mentioned above that should be kept in mind. The *Kepler* results invoked in the previous paragraph are still preliminary, and although we regard our use of them to be conservative for the reasons described earlier, the true fraction of false positives in the *Kepler* sample remains unknown until all candidates have been followed up. The Doppler results are also preliminary to some degree and are based on somewhat limited samples of stars. It is also possible that a fraction of those Doppler candidates may turn out to be false positives, or given the $\sin i$ ambiguity inherent in that technique, that some of them may have actual masses above the range considered for super-Earths. Additionally, there are uncertainties associated with the conversion we have applied between planetary masses and planetary radii, using theoretical models. Those uncertainties are difficult to quantify given our present state of knowledge.

For these reasons, added to the fact that despite our best efforts to assess the BF there could still be some exotic blend scenario that we have overlooked, it is not possible to present a more definitive value of the FAR. Nevertheless, the above estimates of the FAR based on consideration of all the blend scenarios that seem plausible to us are all sufficiently small that they give us very high confidence that KOI-377.03 is not a false positive, and they therefore validate it as a signal of planetary origin. We designate this planet Kepler-9 d.

4. DISCUSSION

Calculating the FAR for targets with small signals such as Kepler-9 d is non-trivial because it depends crucially on the frequency of small transiting planets, which may only be fully known at the conclusion of the *Kepler* Mission. Of the arguments for the expected value of N_p presented in the previous section, the one that relies on the preliminary *Kepler* results themselves is the most conservative, and already makes it highly unlikely that

Table 8
Derived Properties of Kepler-9 d

Parameter	Value[a]
Orbital period (days)	1.592851 ± 0.000045
Mid-transit epoch (BJD)	$2{,}455{,}015.0943^{+0.0018}_{-0.0033}$
Orbital semimajor axis (AU)	$0.02730^{+0.00042}_{-0.00043}$
Transit duration (hours)[b]	$1.97^{+0.13}_{-0.17}$
$R_p/R_\star$	$0.0147^{+0.0015}_{-0.0011}$
R_p ($R_\oplus$)	$1.64^{+0.19}_{-0.14}$
$a/R_\star$[c]	$5.54^{+0.51}_{-2.36}$
Equilibrium temperature (K)[d]	2026 ± 60

Notes.
[a] Values and uncertainties correspond to the mode and 1σ confidence levels derived from the a posteriori distributions generated with the Markov Chain Monte Carlo algorithm.
[b] Defined here as the time interval between the first and last contacts.
[c] The calculation of the normalized semimajor axis assumes that the orbit is circular.
[d] Zero-albedo equilibrium temperature ignoring the energy redistribution factor.

we are in the presence of a false positive such as those explored in this paper. Furthermore, that estimate is based on results from only the first $\sim$43 days of operation of the spacecraft. Continued observations over the next two years will surely increase the number of candidates, which can only result in a larger confidence that the 1.6 day photometric signal is due to a true planet. Thus, we find the overall evidence for the planet interpretation very compelling. It is also worth noting that the Doppler surveys have found that a very large fraction of the smallest-mass planetary companions (as many as 80%) are in multi-planet systems (e.g., Lovis et al. 2008; Mayor et al. 2009). Because of the presence of Kepler-9 b and c, this makes it considerably more likely that Kepler-9 d is also a planet than if it were the only signal in the system. Furthermore, one may expect a priori that a planet interior to Kepler-9 b and c would have a high probability of presenting transits. Indeed, with the reasonable assumption that the orbit of the inner planet is more or less coplanar with the outer two, the geometric probability of a transit at a period of 1.6 days would be close to 100%, instead of $\sim$18% for random inclinations.

The light-curve parameters we obtain for Kepler-9 d by modeling the photometry using the formalism of Mandel & Agol (2002) are summarized in Table 8, and supersede the preliminary estimates of Holman et al. (2010). The values and uncertainties were determined using a Markov Chain Monte Carlo technique, with four chains of length 10^6 each. Our fits used the non-linear fourth-order limb-darkening law of Claret (2000), with coefficients for the *Kepler* band taken from the calculations by A. Prsa referenced in footnote 23. For an adopted stellar radius for the primary star of $R_\star = 1.02 \pm 0.05\,R_\odot$, the estimated size of this planet is $R_p = 1.64^{+0.19}_{-0.14}\,R_\oplus$, which is among the smallest yet reported.[28] The uncertainly is currently dominated by the photometric errors, rather than the stellar parameters, and should improve as more measurements are gathered. The impact parameter of Kepler-9 d is very poorly constrained by

---

[28] The size of Kepler-9 d is not significantly different from that of *CoRoT*-7 b, which is $R_p = 1.68 \pm 0.09\,R_\oplus$ according to Léger et al. (2009) and was revised to $R_p = 1.58 \pm 0.10\,R_\oplus$ by Bruntt et al. (2010). The measured radius of the next smallest known planet, GJ 1214 b, is $R_p = 2.68 \pm 0.13\,R_\oplus$ (Charbonneau et al. 2009).

current data, but should also become better determined in the future. A mass determination for this object has not been made, and will be challenging given the small amplitude expected for the reflex motion of the star. The radial-velocity semi-amplitude would be only about 2.3 m s^{-1} assuming a similar mean density as the Earth. Velocity measurements are further complicated by the presence of the other two planets in this system.

Many of the most interesting candidates found by *Kepler* will correspond to Earth-size planets, some of which are expected be in the habitable zone of their host star. For solar-type stars this implies reflex motions with radial-velocity amplitudes below current detection limits, making the spectroscopic measurement of the mass impossible. Other reasons may also hinder this type of validation, such as rapid rotation, chromospheric activity, or even the faintness of the star.

The information contained in the *Kepler* light curves on the shape of a transit-like event is a valuable asset for constraining the vast range of possible astrophysical false positives that might be masquerading as a planet. Here, we have shown how modeling the light curve of a candidate directly as a false positive allows to rule out a significant fraction of blends involving background or foreground eclipsing binaries or star–planet pairs, as well as hierarchical triple systems, each of these possibly attenuated by the light of additional stars. The combination of BLENDER with follow-up observations consisting of high-resolution imaging, spectroscopy, and an analysis of the centroid motion of the target leaves no room for a false positive in the case of Kepler-9 b and c. These signals were previously known to correspond to bona fide Saturn-size planets because they display correlated TTVs (Holman et al. 2010). Nevertheless, the exercise serves to show that, lacking that evidence, it would still be possible to validate them using the same techniques, thus supporting the general approach and justifying the application to the more interesting Kepler-9 d signal.

Among the advantages of BLENDER for *Kepler* is the ability to predict the brightness and overall color of a blend in many different passbands. Brightness information for virtually every *Kepler* target is available from the KIC in the Sloan *griz* and 2MASS *JHK$_s$* bands, as well as in the custom D51 passband (518.7 nm). We have shown earlier how these can be used to rule out certain blend scenarios that might otherwise be viable. The detailed fitting of the photometry with a false-positive model provides additional discriminating power. Rough estimates of the properties of a background eclipsing binary that can mimic a blend have sometimes been made in previous transit surveys based simply on the apparent brightness of the object and a representative depth for its undiluted eclipses (such as 50%). While such configurations may well reproduce the observed amplitude of a candidate light curve, not much can be said about the expected shape, which may be completely wrong. An example of this is seen for Kepler-9 d in Figure 16, in which a back-of-the-envelope calculation of the depth one might predict from the brightness and ∼50% deep eclipses of this binary may not be far off, but the detailed shape is not a good match to the observations, and BLENDER easily rules out this scenario giving a poor χ^2 for the fit. Without these additional constraints on blend properties provided by the detailed light-curve fitting, the space of parameters open to false positives would be significantly larger and more difficult to exclude by other means.

REFERENCES

Bakos, G. Á., et al. 2007, ApJ, 670, 826
Batalha, N. M., et al. 2010, ApJ, 713, L103
Borucki, W. J., et al. 2010, Science, 327, 977
Borucki, W. J., et al. 2011, APJ, in press (arXiv:1006.2799)
Bruntt, H., et al. 2010, A&A, 519, A51
Bryson, S. T., et al. 2010, ApJ, 713, L97
Cardelli, J. A., Clayton, C., & Mathis, J. S. 1989, ApJ, 345, 245
Charbonneau, D., et al. 2009, Nature, 462, 891
Claret, A. 2000, A&A, 363, 1081
Etzel, P. B. 1981, in Photometric and Spectroscopic Binary Systems, ed. E. B. Carling & Z. Kopal (Dordrecht: Reidel), 111
Fressin, F., Guillot, T., Morello, V., & Pont, F. 2007, A&A, 475, 729
Fressin, F., Guillot, T., & Nesta, L. 2009, A&A, 504, 605
Gilliland, R. L., et al. 2010, ApJ, 713, L160
Hayward, T. L., Brandl, B., Pirger, B., Blacken, C., Gull, G. E., Schoenwald, J., & Houck, J. R. 2001, PASP, 113, 105
Holman, M. J., et al. 2010, Science, 330, 51
Howard, A. W., et al. 2010, Science, 330, 653
Ida, S., & Lin, D. N. C. 2004, ApJ, 604, 388
Jenkins, J. M., et al. 2010, ApJ, 724, 1108
King, I. R. 1983, PASP, 95, 163
Kipping, D. M. 2010, MNRAS, 408, 1758
Koch, D. G., et al. 2010, ApJ, 713, L79
Latham, D. W., Brown, T. M., Monet, D. G., Everett, M., Esquerdo, G. A., & Hergenrother, C. W. 2005, BAAS, 207, 110.13
Léger, A., et al. 2009, A&A, 506, 287
Lovis, C., Mayor, M., Bouchy, F., Pepe, F., Queloz, D., Udry, S., Benz, W., & Mordasini, C. 2008, in IAU Symp. 253, Transiting Planets, ed. F. Pont, D. Sasselov, & M. Holman (Cambridge: Cambridge Univ. Press), 502
Mandel, K., & Agol, E. 2002, ApJ, 580, L171
Mandushev, G., et al. 2005, ApJ, 621, 1061
Marigo, P., Girardi, L., Bressan, A., Groenewegen, M. A. T., Silva, L., & Granato, G. L. 2008, A&A, 482, 883
Mayor, M., et al. 2009, A&A, 507, 487
Mazeh, T. 2008, in Tidal Effects in Stars, Planets and Disks, ed. M.-J. Goupil & J.-P. Zahn (EAS Publications Series Vol. 29; Les Ulis: EDP Sciences), 1
Monet, D. G., Jenkins, J. M., Dunham, E. W., Bryson, S. T., Gilliland, R. L., Latham, D. W., Borucki, W. J., & Koch, D. G. 2010, arXiv:1001.0305
Mordasini, C., Alibert, Y., & Benz, W. 2009, A&A, 501, 1139
Nelson, B., & Davis, W. 1972, ApJ, 174, 617
O'Donovan, F. T., et al. 2006, ApJ, 644, 1237
Popper, D. M., & Etzel, P. B. 1981, AJ, 86, 102
Prsa, A., et al. 2011, AJ, in press (arXiv:1006:2815)
Queloz, D., et al. 2001, A&A, 379, 279
Robin, A. C., Reylé, C., Derriére, S., & Picaud, S. 2003, A&A, 409, 523
Sing, D. K. 2010, A&A, 510, 21
Steffen, J. H., et al. 2010, ApJ, 725, 1226
Torres, G., Konacki, M., Sasselov, D. D., & Jha, S. 2004, ApJ, 614, 979
Torres, G., Konacki, M., Sasselov, D. D., & Jha, S. 2005, ApJ, 619, 558
Valencia, D., Sasselov, D. D., & O'Connell, R. J. 2007, ApJ, 656, 545
Vogt, S. S., et al. 1994, Proc. SPIE, 2198, 362
Zacharias, N., Urban, S. E., Zacharias, M. I., Wycoff, G. L., Hall, D. M., Monet, D. G., & Rafferty, T. J. 2004, AJ, 127, 3043